



biblio.ugent.be

The UGent Institutional Repository is the electronic archiving and dissemination platform for all UGent research publications. Ghent University has implemented a mandate stipulating that all academic publications of UGent researchers should be deposited and archived in this repository. Except for items where current copyright restrictions apply, these papers are available in Open Access.

This item is the archived peer-reviewed author-version of: Influence of extended dwell time during pre- and main compression on the properties of ibuprofen tablets

Authors: Peeters E., Silva A.F.T., Fonteyne M., De Beer T., Vervaet C., Remon J.P.

In: European Journal of Pharmaceutics and Biopharmaceutics, 128: 300-315

To refer to or to cite this work, please use the citation to the published version:

Peeters E., Silva A.F.T., Fonteyne M., De Beer T., Vervaet C., Remon J.P. (2018) Influence of extended dwell time during pre- and main compression on the properties of ibuprofen tablets

European Journal of Pharmaceutics and Biopharmaceutics, 128: 300-315

DOI: [10.1016/j.ejpb.2018.05.007](https://doi.org/10.1016/j.ejpb.2018.05.007)

1 **Influence of extended dwell time during pre- and main compression on the properties**
2 **of ibuprofen tablets**

3 E. Peeters^a, A.F.T. Silva^{b,1}, M. Fonteyne^b, T. De Beer^b, C. Vervaet^a, J.P. Remon^a

4
5 ^a Ghent University, Faculty of Pharmaceutical Sciences, Campus Heymans, Laboratory of
6 Pharmaceutical Technology, Ottergemsesteenweg 460, 9000 Ghent, Belgium.

7 ^b Ghent University, Faculty of Pharmaceutical Sciences, Campus Heymans, Laboratory of
8 Pharmaceutical Process Analytical Technology, Ottergemsesteenweg 460, 9000 Ghent,
9 Belgium.

10 ¹ IAQV/REQUIMTE, Department of Chemical Sciences, Faculty of Pharmacy, University of
11 Porto, Rua Jorge Viterbo Ferreira, 228, 4050-313 Porto, Portugal.

12
13 E. Peeters: Elisabeth Peeters, PhD student, Elisabeth.Peeters@Pfizer.com

14 A.F.T. Silva: Ana Filipa Tavares da Silva, PhD student, Ana.TavaresdaSilva@UGent.be

15 M. Fonteyne: Margot Fonteyne, PhD student, Thomas.DeBeer@UGent.be

16 T. De Beer: Thomas De Beer, Professor, Thomas.DeBeer@UGent.be

17 C. Vervaet: Chris Vervaet, Professor, Chris.Vervaet@UGent.be

18 J.P. Remon: Jean-Paul Remon, Professor, JeanPaul.Remon@UGent.be

19
20 **Corresponding Author**

21
22 Chris Vervaet

23 Ghent University - Faculty of Pharmaceutical Sciences

24 Campus Heymans

25 Laboratory of Pharmaceutical Technology

26 Ottergemsesteenweg 460

27 9000 Ghent

28 Belgium

29 Tel: 0032 9 264 80 69

30 Fax: 0032 9 222 82 36

31 E-mail: Chris.Vervaet@UGent.be

32

33

34 **Abstract**

35

36 The low melting point, poor flow, physico-mechanical properties (particle size distribution,
37 shape, particle surface roughness) and deformation mechanism of ibuprofen in combination
38 with its high dose in tablets all contribute to the problems observed during the compaction of
39 ibuprofen-based formulations. Since ibuprofen is plastically and elastically deforming, the rate
40 of compaction plays an important role in both the final tablet properties and the risk of capping,
41 laminating and sticking to the punches. While the compaction rate in most tableting machines
42 is only determined by the tableting speed, the high speed rotary tableting machine used in this
43 research project (MODUL™ P, GEA Process Engineering, Halle, Belgium) can adjust and
44 control the dwell time independently from the tableting speed, using an air compensator which
45 allows displacement of the upper (pre-) compression roller. The effect of this machine design
46 on process parameters and tablet properties was investigated. Granules containing 80%
47 ibuprofen were compressed into tablets at 250, 500 and 1000 tablets per minute via double
48 compression (pre- and main compression) with or without extended dwell time. Prior to
49 tableting, granule properties were determined. Process parameters and tablet properties were
50 analyzed using Multivariate Data Analysis. Principal Component Analysis provided an
51 overview of the main phenomena determining the tableting process and Partial Least Squares
52 Analysis unveiled the main variables contributing to the observed differences in the tablet
53 properties.

54

55 **Keywords**

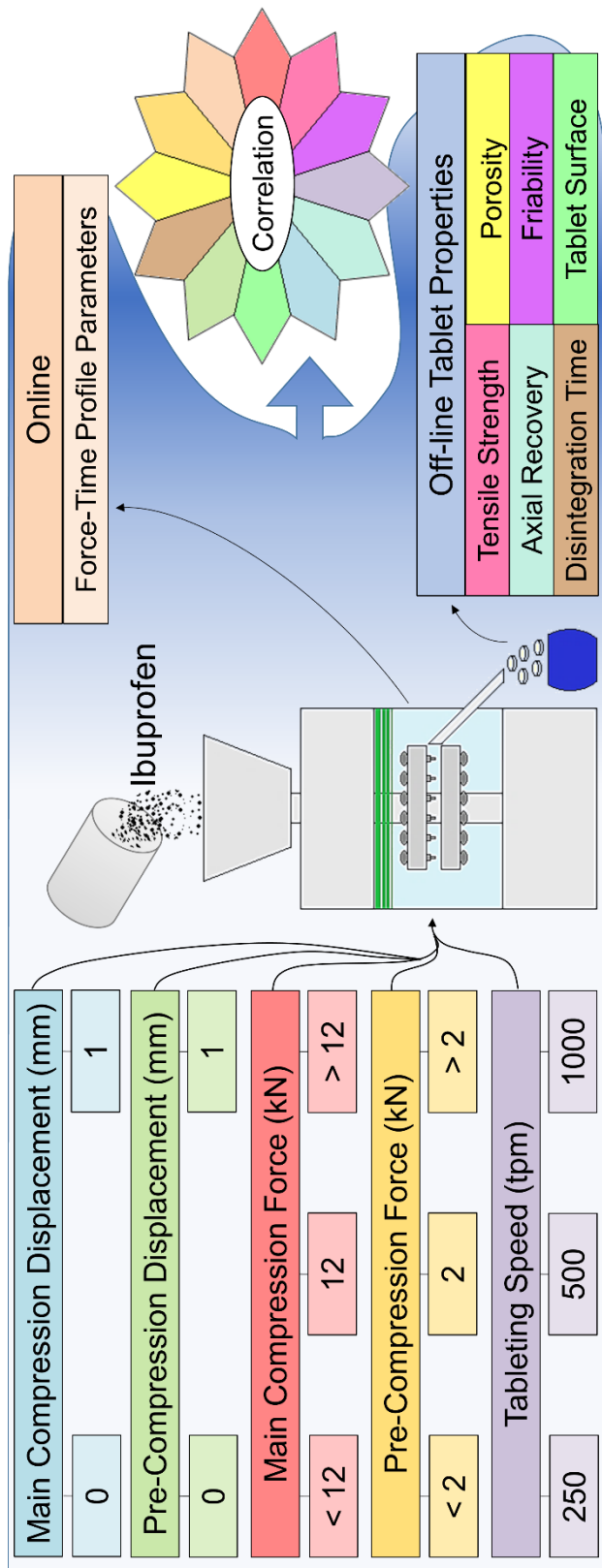
56

57 Tableting, Rotary tablet press, Displacement, Force-Time profile, Extended dwell time,
58 Multivariate data analysis.

59

60

61



63 1. Introduction

64

65 Ibuprofen is widely used for the treatment of rheumatoid arthritis, osteoarthritis and mild and
66 moderate pain, in daily doses ranging from 0.2 to 2.4 g [1]. For high-dosed tablets, the physico-
67 mechanical properties of the pure component play a major role in the tableting process [2, 3].
68 As a result, the processing of ibuprofen into tablets still encounters problems due to its low
69 melting point, poor flow and deformation mechanism [3-5]. Various attempts were made to
70 improve the tableting behavior of ibuprofen formulations (flowability, tableability,
71 compactibility) by recrystallization, dry granulation (roller compaction, pressure swing
72 granulation) or dry coating [3-11]. Although these methods contribute to the understanding of
73 the tableting behavior of ibuprofen, the applicability in production settings is limited, due to the
74 rather moderate improvements and long processing times of some methods.

75

76 Since the common crystal form (needle-like shape) of ibuprofen undergoes plastic and elastic
77 deformation, the rate of compaction plays an important role in both the final tablet properties
78 and the risk of capping, laminating and sticking to the punches [2, 12, 13]. Besides the
79 compaction rate, also the punch tip geometry, embossment [14] and roughness, as well as
80 the composition of the punch tip coating (i.e. boron-alloy, chrome, ...) [15] have an influence
81 on the sticking tendency. Consequently, in industrial manufacturing the production process is
82 optimized either by optimizing the tooling, or reducing the rate of compaction, or both [2, 12-
83 15].

84

85 In most tableting machines, the compaction rate (i.e. consolidation phase, dwell time,
86 decompression phase) can only be adjusted by changing the tableting speed [16]. However,
87 using the MODUL™ P high-speed rotary tablet press (GEA Process Engineering, Halle,
88 Belgium) the dwell time can be adjusted and controlled independently of the tableting speed,
89 due to an air compensator which allows displacement of the upper (pre-) compression roll.
90 This design, which has not yet been thoroughly described in literature, could affect the

91 processability of materials exhibiting a rate-dependent compression behavior, like ibuprofen
92 [2, 12, 13, 17].

93

94 The aim of this study was to get a thorough understanding of this compression method (i.e.
95 speed-independent extended dwell time). Using a commercial ibuprofen formulation, the
96 influence of extended dwell time independent of compression speed on the dependent
97 machine parameters and on the tablet properties was examined. Due to the large amount of
98 data obtained (process parameters and tablet characteristics), multivariate data analysis was
99 used to analyze and present results in a structured manner.

100

101 **2. Materials and methods**

102

103 **2.1. Materials**

104

105 Granules, containing 80 % ibuprofen, were kindly donated by Sanico (Turnhout, Belgium), and
106 used as received. The granules were produced by fluid bed wet granulation. A premixed blend
107 of the active pharmaceutical ingredient (API) and a binder were agglomerated with water as
108 the granulation liquid. After drying, a glidant, lubricant and anti-adhesive were added
109 externally.

110

111 **2.2. Granule characterization**

112

113 Particle size analysis was done by sieve analysis ($n = 3$), using a sieve shaker (Retsch VE
114 1000, Haan, Germany). 200 g of granules was placed on a nest of sieves (50, 100, 150, 250,
115 300, 500, 710, 1000 and 1120 μm) and shaken at an amplitude of 2 mm for 10 min. The
116 amount of granules retained on each sieve was determined. The density (ρ_{true}) of the granules
117 was measured ($n = 3$) using a helium pycnometer (Accupyc 1330 pycnometer, Micrometrics
118 Instruments, Norcross, Georgia, USA), with ten purges and ten runs per measurement. The

119 bulk (ρ_{bulk}) and tapped density (ρ_{tapped}) of 30 g of granules was determined in a 100 ml
120 graduated cylinder ($n = 3$). The powder was poured from a height of 40 cm through a stainless
121 steel funnel with a 10 mm orifice into the graduated cylinder, mounted on a tapping device (J.
122 Engelsmann, Ludwigshafen am Rhein, Germany). Bulk and tapped densities were calculated
123 as $30 \text{ g}/V_0$ and $30 \text{ g}/V_{1250}$, respectively. These values were used to calculate the
124 compressibility index (CI) in order to assess the tendency of a powder to consolidate [18].

125

126 **2.3. Preparation of tablets**

127

128 **2.3.1. Mechanism of compression**

129

130 All tablets were prepared by double compression (i.e. a pre-compression and main
131 compression step). At the pre-compression station the punches apply an initial force on the
132 powder, and subsequently, under the main compression rollers the final compression takes
133 place, usually at a higher load compared to the pre-compression phase [19-21]. The role of
134 the pre-compression step is to reduce air-entrapment during the main compression step. Also
135 the extent of stress-relaxation is increased by effectively extending the dwell time via pre-
136 compression, yielding stronger tablets [20-23].

137

138 Most rotary tablet presses operate by maintaining fixed roller positions during compression.
139 The upper roller remains in a fixed position, which determines the penetration depth of the
140 upper punch and consequently the in-die tableting position. By adjusting the position of the
141 lower roller, the compression force is determined and hence, the thickness of the compact
142 under compression. Furthermore, for a given tablet press and tooling, the kinetics of the punch
143 movement depend only on the tableting speed. As a result the total contact time (the period
144 when the upper punch is in contact with the powder), the consolidation time (the period during
145 which the punches approach each other), the dwell time (the period during which the punch
146 head flat is in direct contact with the compression roller), the decompression phase (the time

147 during which the punches move away from each other) and the lag-time (the time between
148 pre-compression and main compression phase) are defined by the tangential velocity of the
149 punch [16, 20-22, 24-37].

150

151 In contrast, using the MODUL™ P high-speed rotary tablet press these parameters can be
152 controlled independently from the tableting speed, due to an air compensator which allows
153 displacement of the upper compression rollers (Figure 1). The upper rollers are attached to
154 an air piston, which allows vertical movement in an air cylinder. During a compression run the
155 air pressure in the cylinder (CF_r) is set at a constant value due to a control system of pressure
156 valves and expansion vessels. The piston, and consequently the upper roller, is pushed
157 downwards by the air pressure against a fixed stop, being the bottom of the air cylinder. The
158 adjustable position of the lower roller is controlled similar to a conventional tablet press with
159 fixed rollers. During compression, the upper punch initially moves downwards into the die
160 when in contact with the upper roller. As the lower punch is pushed upwards by the lower
161 roller, the powder bed in the die consolidates and the compression force increases. When the
162 reaction force exerted by the powder on the upper punch exceeds the force exerted by the
163 counter pressure (i.e. the air pressure on the piston), upward movement of the upper
164 compression roller is possible. The complete assembly of bottom punch, powder slug and top
165 punch moves simultaneously, following the lower compression roller and consequently raises
166 the upper roller. The distance by which the upper roller is displaced only depends on the
167 position of the lower compression roller. The dwell time is now not only defined by the punch
168 head flat, the pitch diameter and the turret speed, but also by the displacement. As the upper
169 roller is displaced, the contact time between the punch head flat and the roller is prolonged.
170 Hence the dwell time is extended in comparison to the fixed roller set-up, although tableting
171 speed is constant. If, however, a higher air pressure than the force exerted by the powder is
172 set in the cylinder of the air compensator, the upper roller does not move, and the system
173 behaves as a set-up with fixed rollers [17].

174

175 This system with moving rollers has major implications on the control systems and kinetics of
176 punch movement, compared to a system with fixed rollers. The shape of the force-time
177 profiles, and mainly the dwell time, is affected, as further discussed in more detail [17, 19, 28,
178 32]. Another implication of this concept is the effect on the in-die tableting position since the
179 lower roller will have a higher position in order to induce displacement. Therefore, the position
180 of the powder slug in the die will be higher compared to a system with fixed rollers. Hence the
181 distance travelled by the tablet before being ejected is less which can influence the stress
182 applied on the powder bed, resulting in a different relaxation behaviour [22]. A schematic
183 overview of the different positions and movements of rollers and punches is provided in Figure
184 2.

185

186 It is necessary to mention that the term 'displacement' in this research is strictly used to
187 describe *the movement of the upper roller*, and *not* the movement of the punches, as it is done
188 in all previous research describing force-time profiles.

189

190 **2.3.2. Collection of data**

191

192 The tablet press is equipped with strain gauge-based load cells which are used for force
193 measurement at pre- and main compression and at ejection. Load cells below the lower
194 compression rollers and the ejection cam measure the compression force (CF) and ejection
195 force (EF), respectively. Displacement of pre- and main compression rollers is measured by
196 linear variable displacement transducers (LVDT sensors), which are connected to the upper
197 compression rollers. Punch stroke movement is monitored by LVDT sensors, which are placed
198 inside the turret and are fixed to one keyed punch set by means of clamps.

199

200 Collection and analysis of the data was performed with a data acquisition and analysis system
201 (CDAAS) (GEA Process Engineering, Halle, Belgium). The CDAAS software is an application
202 which measures and samples the signals (pre-compression force (PCF), main compression

203 force (MCF), pre-compression displacement (PCD), main compression displacement (MCD),
204 ejection force (EF) and punch strokes) at high frequency (up to 100 kHz) with 16bit A/D
205 conversion. It allows calibration, filtering, visualization and recording of the processed sensor
206 signals and reviewing and analyzing of recorded data.

207

208 **2.3.3. Tableability**

209

210 In order to determine the MCF at which the experiments should be performed, a preliminary
211 tableability study was performed. Tableability may be defined as the capacity of a powder to
212 be transformed into a tablet of specified strength under the effect of compaction pressure. It
213 can be represented by a plot of tensile strength (TS) versus compaction pressure [30, 35, 38-
214 41]. Although very useful, the obtained correlation is not an intrinsic material characteristics
215 and the profile is dependent upon the press, tooling and settings used (e.g. tableting speed,
216 paddle speed in the forced feeder, fill depth) [30, 31, 35, 40]. Therefore, the same tooling ($n =$
217 10, standard euro B, diameter 12 mm, concave radius 24 mm) was used throughout the study.
218 The fill depth was adjusted to obtain tablets of 500 mg, in accordance with the dwell time
219 experiments. Tableting speed was set at 500 tablets per minute (tpm) and force feeder speeds
220 were kept constant at 25 and 40 rpm. PCF was set at 2 kN and PCD at 0.2 mm. MCD was
221 kept at 0.0 mm for all experiments and MCF was varied from 3 to 30 kN with increments of 3
222 kN. An extra point at 42 kN MCF was added to examine the TS at a very high compression
223 load. For each experiment the machine was run for 2 minutes, with sampling during the second
224 minute. Room temperature (21.0 ± 2.0 °C) and relative humidity (RH) (30.0 ± 2.0 %) were
225 controlled.

226

227 **2.3.4. Influence of extended dwell time**

228

229 A series of experiments was conducted in order to investigate the effect of the extended dwell
230 time induced by displacement. Experiments were repeated at three different tableting speeds

231 to examine the effect of this parameter. Initially, the experimental set-up consisted of 12
232 experiments, in which three factors were varied (Table 1). PCF was kept constant at 2 kN and
233 MCF was set at 12 kN, based on the results of the preliminary tableability test. However, the
234 shape of the force-time signal for tablets compressed with moving rollers induced some set-
235 up modifications, as this profile deviated from the theoretical profile (Figure 3) [35]. This
236 atypical shape is caused by the inertia of the system and is inherently correlated to the design
237 of the air compensator. A limited “overshoot” occurs before the plateau of the extended dwell
238 is reached. Furthermore, the ratio between F_{top} and $F_{mplateau}$ (defined as the mean value of
239 F_{25dw} , F_{50dw} and F_{75dw} (see further)) increases at higher tableting speed, which is by default due
240 to the larger impact at higher punch velocities when the punches come into contact with the
241 compression rollers. As a result, two compression forces (F_{top} and $F_{mplateau}$) were taken into
242 account for analysis and correlation with the tablet properties. Hence, PCF and MCF values
243 of 2 kN and 12 kN, respectively, were maintained, in order to be able to compare the
244 experiments between different tableting speeds. Moreover, depending on the tableting speed,
245 the other compression force (with displacement) was determined as the resulting F_{top} by
246 keeping the $F_{mplateau}$ on these preset values (i.e. experiment 3 in Figure 4). This ultimately
247 resulted in an adjusted set-up with seven experiments per tableting speed (total of 20
248 experiments, experiment 12 was not performed), from which a schematic overview is provided
249 in Figure 4. The red bars indicate the set PCF and MCF of 2 and 12 kN respectively. However,
250 when this bar is not located at the top of the curve (F_{top}), this indicates that the powder bed is
251 actually exposed to a higher compression force during compression.

252

253 Tablets were prepared on the MODUL™ P, equipped with an overfill cam of 16 mm and using
254 a set of punches as described earlier. The fill depth was adjusted prior to each experiment to
255 obtain tablets of 500 mg. Tableting speed was set at 250, 500 or 1000 tpm, depending on the
256 experiment. As paddle speed must be adjusted in function of tableting speed in order to avoid
257 speed-induced weight variability [42], force feeder speeds were set either at 10 rpm – 50 rpm,
258 25 rpm – 40 rpm or 35 rpm – 50 rpm. PCF, PCD, MCF and MCD were set according to the

259 experiment (Figure 4). In order to avoid confounding factors, each experiment was run on an
260 empty and cleaned tablet press. The machine was run for 2 minutes, with sampling during the
261 second minute. Room temperature (21.0 ± 2.0 °C) and relative humidity (30.0 ± 2.0 %) were
262 controlled. A summary of the machine settings is given in Table 2.

263

264 **2.4. Data analysis**

265

266 **2.4.1. Analysis of process parameters**

267

268 The CDAAS software stores the collected data from the seven signals as a continuous
269 recording, with time (msec) on the X-axis. PCF, MCF and EF are plotted on one Y-axis (kN),
270 whereas PCD, MCD, movement of bottom punch and movement of upper punch are plotted
271 against distance (mm) (Figure 5).

272

273 Force-time profiles are already thoroughly addressed by other authors [16, 32-34, 36, 37].

274 Although these researchers provided insight and proposed applicable evaluation methods for
275 force-time profiles on rotary tablet presses, all these studies were conducted with a fixed roller
276 set-up. Consequently, the moving roller assembly used in this research and the resulting
277 atypical force-time profile requires a modified analysis protocol. Moreover, since it is possible
278 to compress tablets with both methods (fixed and moving rollers), parameters allowing
279 quantitative comparison between both types of profiles had to be defined. A schematic
280 overview of these parameters is given in Figure 6, which represents a force-time profile without
281 and with displacement (i.e. fixed and moving rollers). Since the shape of the force-time profile
282 without displacement was slightly different for main compression compared to pre-
283 compression, a representation of both (Figure 6a and 6b) is provided. The force-time profiles
284 with displacement were comparable for both stations (Figure 6c).

285

286 First, the contact time (t_{total} , from t_{begin} to t_{end}) and the area under the curve of the complete
287 profile (AUC_{total}) were defined as parameters [16, 33, 34]. Subsequently, the force-time profile
288 was divided into three phases: the consolidation phase, the dwell time and the decompression
289 phase [16, 33, 34, 36]. The method used to define these phases on the force-time curves
290 depended if the run was performed with fixed or moving rollers. Using moving rollers, the onset
291 and end of the displacement-time signal clearly marked the beginning and end point of the
292 dwell time. This also allowed easy tracking of the consolidation and decompression phase. In
293 runs with fixed rollers, there is no signal indicating when the punches are vertically aligned
294 with the center of the pressure role. For each tableting speed (250, 500 and 1000 tpm) five
295 consecutive force-time signals of the first run (experiment 1 in Figure 4, pre- and main
296 compression without displacement) were aligned on the X-axis by means of an algorithm with
297 five consecutive force-time signals of the second run (experiment 2 in Figure 4, pre- and main
298 compression with displacement). As the middle of the displacement-time signal of experiment
299 2 marks the center of the compression role, by default it also marks the middle of the dwell
300 time on the force-time profile for both aligned experiments. Knowledge about the middle of the
301 dwell time (t_{50dw}) allows correct positioning of the dwell time on the force-time profile. The dwell
302 time (t_{dw}) (msec) itself, for the force-time signals without displacement, was calculated
303 according to Equation (1) [43]:

304

$$305 \quad t_{dw} = \frac{6 \times 10^4 \times R_h}{\pi \times \omega \times R_p} \quad (1)$$

306

307 Where R_h , R_p and ω denote the radius of the punch head flat (mm), half of the pitch circle
308 diameter of the turret (mm) and the turret speed (rpm), respectively.

309

310 In order to allow a faster determination of t_{50dw} for the other experiments without displacement,
311 an empirical method was derived. For main compression, the dwell time of the force-time
312 profiles without displacement were characterized by the same force at the beginning of the

313 dwell time (F_{bdw}) as at the end (F_{edw}) (Figure 6a). Therefore, the onset and end of the dwell
314 time were defined by the intersections between the force-time profile and a horizontal line with
315 a length equal to the theoretical calculated dwell time. For pre-compression, the endpoint of
316 the dwell time on the force-time profile without displacement was characterized by a rather
317 sudden and sharp drop in the force profile (F_{edw}) (Figure 6b). Consequently, the onset of the
318 dwell time was determined based on this sharp decrease of the force using a line parallel to
319 the X-axis with a length equal to the theoretical dwell time.

320

321 Next to the dwell time (t_{dw}), the middle of the dwell time (t_{50dw}) and the forces at the beginning
322 and the end of the dwell time (F_{bdw} and F_{edw} respectively), additional parameters for this phase
323 were determined. The force at 25% (F_{25dw}), 50% (F_{50dw}) and 75% (F_{75dw}) of the dwell time and
324 the respectively absolute time-points (t_{25dw} , t_{50dw} , t_{75dw}) were determined. The same procedure
325 was followed for the maximum and minimum force occurring during the dwell time (F_{max} , t_{Fmax} ;
326 F_{min} , t_{Fmin}). The maximum force is also referred to as F_{curve} or F_{top} (Figure 3), depending on
327 compression without or with displacement, respectively. $F_{mplateau}$ was determined as the mean
328 value of F_{25dw} , F_{50dw} and F_{75dw} . Furthermore, a dimensionless parameter describing the shape
329 of the force-time profile, independent of the absolute force values used, was included: the
330 t/p_{mean} ratio was defined as the ratio between F_{max} and $F_{mplateau}$.

331

332 For the consolidation phase, the consolidation time (t_{con} , from t_{begin} to t_{bdw}), the area under the
333 curve (AUC_{con}) and the slope (S_{con}) were defined as parameters. The decompression phase
334 was analyzed accordingly (t_{decomp} , from t_{edw} to t_{end} ; AUC_{decomp} ; S_{decomp}) [16, 24, 33, 34]. As
335 observed in Figure 6, both the consolidation and the decompression phases make up a small
336 portion of the entire profile when displacement is used, characterized by a shorter time span
337 and a steeper slope.

338

339 From the ejection profile (yellow line on Figure 5) only the maximum ejection force (F_{ejec}) was
340 considered.

341

342 As stated above, the displacement-time profiles (red and orange line on Figure 5) were used
343 to measure the dwell time on the force-time profiles. Furthermore, the maximum displacement
344 (CD) was taken into account for further analysis. The signals for bottom punch and top punch
345 movement (blue and purple line on Figure 5) were used to calculate the in-die thickness of the
346 powder plug. The minimum in-die thickness (T_{ID}) was calculated by determining the minimum
347 distance between the bottom and upper punch during compression (h_{BT}), for both pre- and
348 main compression. Furthermore, the distance between the punches immediately after pre-
349 and main compression (T_{AD}) was measured in order to calculate the in-die immediate axial
350 recovery (IAR) of the material after each compression step. The point at which the
351 measurement was performed was determined by simultaneously taking into account the
352 punch stroke profile (movement of the punches) and the force-time profile of the same punch.
353 This point was determined as the point immediately after the force dropped to zero and the
354 punches stopped following the movement of the compression rollers. Finally, based on the
355 movement of the bottom punch, the time between the end of punch movement at pre-
356 compression and the beginning of punch movement at main compression was defined as the
357 lag-time (t_{lag}) [20, 21].

358

359 For each run, consecutive force-time ($n = 10$), displacement-time ($n = 10$) and punch motion
360 ($n = 3$) signals were analyzed. Data were then exported for further statistical pretreatment and
361 computations prior to PCA analysis. A schematic overview of all parameters is given in Table
362 3.

363

364 **2.4.2. Tablet evaluation**

365

366 An overview of the examined tablet characteristics is provided in Table 4. In order to obtain
367 information about the influence of the tableting parameters on the granules both “in-die” as
368 well as “out-of-die”, tablet evaluation was done immediately after production (t_0) and after a

369 storage period of seven days (t_7). Friability, disintegration and SEM were only performed after
370 the storage period. Tablets were stored in open tablet trays in a sealed container at $23.1 \pm$
371 1.0 °C and 30.0 ± 2.0 % relative humidity (using a saturated solution of magnesium chloride
372 hexahydrate (Fagron, Waregem, Belgium)).

373

374 Tablets ($n = 10$) were weighed and their hardness, thickness and diameter was determined
375 (Sotax HT 10, Basel, Switzerland). The tablet tensile strength (TS) was calculated using
376 Equation (2) [44].

377

$$378 \quad TS = \frac{2F}{\pi dt} \quad (2)$$

379

380 Where F , d and t denote the diametral crushing force (N), the tablet diameter (mm) and the
381 tablet thickness (mm), respectively.

382

383 Tablet friability was determined on 13 tablets using a friabilator described in the European
384 Pharmacopeia (Pharma Test PTF-E, Hainburg, Germany), at a speed of 25 rpm for 4 min.
385 Tablets were dedusted and weighed prior to and after the test. Tablet friability was expressed
386 as the percentage weight loss. The disintegration time of the tablets ($n = 9$) was evaluated
387 with the Pharma Test PTZ-E (Hainburg, Germany) as described in the European
388 Pharmacopoeia. Tests were performed in distilled water at 37.0 ± 0.5 °C using disks. The
389 disintegration time was determined as the time when no visible particles remained on the mesh
390 wire.

391

392 In order to calculate the porosity (ϵ) of the tablets, the apparent density (ρ_{app}) of the tablets
393 was determined. For the in-die density determination, tablet volume was calculated using
394 Equation (3), according to the diameter of the die, dimensions of the punch tip and the in-die
395 thickness (T_{ID}), derived from the distance between the top and bottom punch (h_{BT}). For out-of-

396 die determination four dimensions of 10 tablets with known weight were measured with a
 397 projection microscope (Reickert, 96/0226, Vienna, Austrich). Subsequently, the volume of the
 398 tablet was calculated according to Equation (3), with D (mm), H (mm), h (mm) and R (mm) the
 399 diameter, the total height determined in the middle, the height of the central cylinder and the
 400 radius of the concave part of the tablet, respectively. Weight divided by the volume of the tablet
 401 resulted in the apparent density (ρ_{app}). Based on the true density of the granules (ρ_{true})
 402 determined by helium pycnometry, the porosity of the tablets was calculated according to
 403 Equation (4).

404

$$405 \quad V = \left[\pi \times \left(\frac{D}{2}\right)^2 \times h \right] + 2 \times \left[\frac{1}{3} \times \pi \times \left(\frac{H-h}{2}\right)^2 \times \left[3 \times R - \left(\frac{H-h}{2}\right) \right] \right] \quad (3)$$

406

$$407 \quad \varepsilon = \left(1 - \frac{\rho_{app}}{\rho_{true}} \right) \times 100 \quad (4)$$

408

409 Several definitions are used to characterize immediate axial tablet expansion or recovery (*IAR*)
 410 (%) [25, 40, 41, 45]. In general, IAR describes the difference between the minimum tablet
 411 thickness under maximum compression force (T_{ID}) (mm) and the tablet thickness after the
 412 pressure is removed (T_A) (mm), as represented by Equation (5) [45].

413

$$414 \quad IAR = \left(\frac{T_A - T_{ID}}{T_{ID}} \right) \times 100 \quad (5)$$

415

416 However, there is a discrepancy between the interpretations of different authors about that
 417 latter data point. Some authors define the tablet height at the end of the decompression phase,
 418 before the tablet is ejected from the die (T_{AD}) [25, 41, 46]. Others measure the tablet thickness
 419 immediately after ejection from the die (T_{i0}) [40, 47] or even after a defined period (e.g. 1
 420 minute) after ejection (T_{tx}) [45, 47]. Since each of these different determinations contributes to
 421 the understanding of the behavior of the granules in the compression cycle, both definitions

422 (before and after ejection) were used in this research. Consequently, three different values of
423 IAR were obtained:

- 424 - IAR_{pre} : the immediate axial recovery after pre-compression, with T_A and T_{ID} the tablet
425 thickness measured in-die immediately after the decompression phase (T_{AD}) and the
426 minimum tablet thickness under maximum pre-compression force, respectively.
- 427 - IAR_{main} : similar to IAR_{pre} , but calculated for the main compression phase.
- 428 - IAR_{t0} : the axial relaxation of the tablet after ejection, where T_A denotes the tablet height
429 immediately after ejection (T_{t0}) and T_{ID} the tablet height under maximum compression
430 force at main compression (T_{IDM}).

431

432 Furthermore, after a recovery period of seven days, the cumulative axial recovery (CAR) was
433 calculated accordingly (Equation (6)) [45]:

434

$$435 \quad CAR = \left(\frac{T_{t7} - T_{IDM}}{T_{IDM}} \right) \times 100 \quad (6)$$

436

437 With CAR the cumulative axial recovery (%), T_{t7} the tablet height after a storage period of
438 seven days (mm) and T_{IDM} the tablet height under maximum compression force at main
439 compression (mm), respectively. Additionally, the hardening of the tablets (%) upon storage
440 was calculated using Equation (7):

441

$$442 \quad Hardening = \left(\frac{TS_{t7} - TS_{t0}}{TS_{t0}} \right) \times 100 \quad (7)$$

443

444 With TS_{t0} and TS_{t7} the tablet tensile strengths (MPa) measured immediately after ejection from
445 the die and after seven days of storage, respectively. In order to simplify the evaluation of the
446 influence of the storage period on the tablet characteristics, a few additional parameters were
447 defined. Diff(CAR-IAR), Diff W, Diff T, Diff D, Diff H and Diff TS represent the changes in axial

448 relaxation, weight, thickness, diameter, hardness and tensile strength of the tablets during
449 storage, respectively.

450

451 SEM was used to study the tablet surface. The tablets were mounted on metal stubs with
452 carbon tape and further processed as described for the granule characterization. The tablets
453 were observed at magnifications of 1000x and 2000x.

454

455 **2.4.3. Multivariate data analysis**

456

457 All calculated mean values and variation coefficients of the machine settings, the data logged
458 by the tablet press and the CDAAS software and the tablet properties were combined in a
459 data table (20 rows, 169 columns) [48]. Principal Component Analysis (PCA) was performed
460 on the machine settings and logged data obtained from the tableting press and CDAAS (*X*,
461 Tables 2 and 3) in order to provide an overview of the performed experiments and investigate
462 the correlations between all process variables. A Partial Least Squares (PLS) regression
463 model was developed to explore the correlations between the machine settings and logged
464 data (*X*) and the tablet properties (*Y*, Table 4). Variables were scaled to unit variance prior to
465 analysis [49]. The multivariate model was developed with the Simca P+ 13 software (Umetrics
466 AB, Umeå, Sweden).

467

468 **3. Results and discussion**

469

470 **3.1. Granule characteristics**

471

472 An overview of the flow properties, true density and particle size distribution of the granules is
473 presented in Table 5. Scanning electron microscope (SEM) pictures (not shown) taken from
474 the material showed that the ibuprofen crystals are needle-like shaped. This observation, in
475 combination with the large fraction of smaller particles detected in the mixture, contributed to

476 the classification of this powder as a fairly flowing powder based on the compressibility index
477 values.

478

479 **3.2. Tableability**

480

481 The influence of MCF on TS is depicted in Figure 7. The TS increases with MCF at
482 compression pressures less than 18 kN. Above 18 kN, the curve gradually levels off to a
483 plateau, where a further increase in the compaction force does not contribute to a higher
484 tensile strength. The higher energy put in the system is not used for additional bond formation
485 and can, in some cases, even decrease the strength of formed bonds, as elastic expansion at
486 higher compression forces is favored [2, 12, 13, 38]. The preferred compression force from a
487 manufacturing point of view is the lowest force (i.e. the least energy input) at which tablets
488 complying with quality- and bioavailability requirements can be produced. The variability in TS
489 however, is significantly larger when a variation (e.g. 0.5 kN) in MCF occurs at lower
490 compression forces, due to the higher slope of the curve at lower compression forces (under
491 10 kN). Since this could be a confounding factor, commonly a force closer to the plateau of
492 the curve is chosen. Consequently, 12 kN was chosen as MCF for further experiments. At this
493 CF, TS still depends on CF and the influence of variation in CF stays rather limited.

494

495 **3.3. Multivariate Data Analysis**

496

497 **3.3.1. Principal Component Analysis**

498

499 Four principal components (PCs) were fitted in the PCA model explaining 81.9% (R^2) of the
500 variation in the data. The first, second, third, and fourth PC explained 29.0%, 24.9%, 19.1%,
501 and 9.8%, respectively.

502

503 Figure 8 depicts the scores of PC1 versus the scores of PC2. Three obvious clusters on the
504 X-axis (PC1) are identifiable: experiments on the left side were performed at a speed of
505 250tpm, on the center at a speed of 500tpm and on the right at a speed of 1000tpm. PC1, the
506 first PC in the model, is found by searching in the multivariate space for the direction of the
507 largest variance. This elucidates again how important the tableting speed is in performing
508 tableting experiments, as it contributes the most to the observed variance. To investigate in
509 detail how the tableting speed is related to the other process parameters, a loading plot is
510 constructed (Figure 9). Scores and loadings have a strong association, and both plots should
511 be observed simultaneously. Observations in a particular place on the score plot have high
512 values for the variables in the same place in the loading plot (positively correlated) and low
513 values for the variables at the opposite site of the loading plot (negatively correlated).
514 Moreover, the effect is more pronounced further away from the origin (i.e. from the middle) of
515 the plot [49]. On the right side of the loading plot (Figure 9), four process variables cluster with
516 the tableting speed (red full circle): fill, S_{con} (P), S_{con} (M) and T_{AD} (M). As tableting speed
517 increases, the fill depth (fill) for powders not exhibiting a free-flowing behavior commonly has
518 to be increased to allow sufficient die filling during the short exposure time to the feeder in
519 order to reach the desired weight. The positive correlation between the after-die thickness
520 (T_{AD}) and the tableting speed confirms the observations of other researchers, who stated that
521 an increased tableting speed is able to increase the immediate elastic expansion [12, 20, 25,
522 27, 40, 50]. S_{con} shows that the tableting speed is closely correlated to the shape of the force-
523 time profile, as this value, representing the slope of the consolidation phase, for both pre- (P)
524 and main compression (M) are significantly increased at high speed. This conclusion is further
525 supported by the cluster situated at the left side of the loading plot, where nearly all other
526 speed related variables of the force-time profile (the area under the curve (AUC) and the
527 different time points (t)) are grouped (red dashed circle). These variables have a higher
528 numerical value when the tableting speed is decreased.

529

530 When looking at the score of PC1 versus the scores of PC2 (Figure 8) along the Y-axis (PC2),
531 two clusters can be distinguished. Loadings for PC2 (Figure 9) show that experiments with a
532 lower score value (lower half of the score plot) were performed at a higher MCD (at the bottom
533 of the loading plot (blue full line)) while experiments with higher PC2 scores (upper half of the
534 score plot) were performed at a lower MCD, which is in accordance with the set-up of the
535 experiments (see also Figure 4). Moreover, experiments with a high score value according to
536 PC2 have a high loading value for MCF_r , M_{bot} and M_{top} as these process parameters can be
537 found at the top of the loading plot, opposite from the MCD (blue dashed circle). This is
538 understandable, as the counterforce in the air compensator (MCF_r) has to be lowered and the
539 position of the lower roller has to be raised (M_{bot} decreased) to allow more upward vertical
540 displacement (MCD) of the compression rollers. Obviously, with displacement, the position of
541 the upper roller will also be raised (M_{top} decreased).

542

543 Several other variables are positively or negatively correlated to MCD as seen on Figure 9
544 (blue dotted circles). Firstly, the inverse correlation between MCD and the ejection force (F_{eject})
545 is an interesting finding worth mentioning. An explanation for this observation can be that with
546 displacement the ejection is facilitated (ejection force lowered), since compression happens
547 higher in the die. Secondly, the model shows the relation between the MCD and the variability
548 of the process. A cluster close to MCD on the loading plot with $VC t_{F_{max}}$, $VC t_{dw}$ and $VC T_{IDM}$
549 highlight that during compression with displacement the variation in dwell time, in the point
550 when maximum force occurs and in in-die thickness is larger than in experiments where no
551 displacement is used. On the opposite side of the loading plot however, a cluster of $VC F_{mplateau}$,
552 $VC F_{max}$ and $VC AUC_{total}$ reveal that the value of these variables is lowered when displacement
553 is used. From these observations can be concluded that during compression with the moving
554 roller set-up, the variability in the process is not translated into variability in the force exerted
555 on the powder bed, as is the case with the fixed roller set-up.

556

557 Finally, the parameters positioned in the left lower corner of the loading plot are positively
558 correlated to the MCD. From this can be concluded that during the experiments with
559 displacement the compression event is statistically prolonged, as the total contact time (t_{total}),
560 the dwell time (t_{dw}) and related values (AUC_{total} , t_{25dw} , t_{50dw} , t_{75dw} , t_{Fmin}) are increased. In
561 contrast, t_{Fmax} can be found at the upper part of the loading plot, so negatively correlated with
562 an increased displacement. This observation becomes clear when looking at the difference in
563 shape of the force-time profile with and without displacement (Figure 6a and Figure 6c). For
564 all former parameters (t_{25dw} , t_{50dw} , t_{75dw} , t_{Fmin}) the difference between that data point and the
565 beginning of the dwell time (t_{bdw}) becomes larger when using displacement. For the latter (t_{Fmax})
566 exactly the opposite effect can be seen. The fact that these process parameters are located
567 on the loading plot more to the left instead of center bottom, indicates that both the tableting
568 speed (PC1) and the displacement at main compression (PC2) are correlated with these
569 parameters. This means that the influence of MCD will be more elucidated at lower tableting
570 speeds. A similar conclusion can be drawn when looking at the position of t/p_{mean} on the
571 loading plot. As it is located closer to the lower right corner, both a higher tableting speed and
572 a higher displacement contribute to this value. As mentioned previously, the atypical shape of
573 the force-time profile with displacement is caused by the inertia of the system and is inherently
574 correlated to the design of the air compensator. Furthermore, the ratio between F_{top} and
575 $F_{mplateau}$ increases at higher tableting speed, which is by default due to the larger impact at
576 higher punch velocities when the punches come into contact with the compression rolls. From
577 this can be concluded that the t/p_{mean} ratio is a sensitive parameter to describe the shape of
578 the force-time profile within the range of the parameter setting used.

579

580 Figure 10 depicts the scores of PC3 versus the scores of PC4 and accordingly, Figure 11
581 represents the loadings of PC3 versus the loadings of PC4. According to PC3 there are two
582 obvious clusters which by looking at the loadings plots can be attributed to differences in the
583 PCD. Experiments with a lower score value (left side of the score plot) were performed at a
584 higher PCD (left side of the loading plot (blue full line)) while experiments with higher PC3

585 scores (right side of the score plot) were performed at a lower PCD, which is also in
586 accordance with the set-up of the experiments (see also Figure 4). Some of the observed
587 relations show similarity with those observed between the score and loading plot according to
588 PC2. For instance, experiments with a high score value according to PC3 have a high loading
589 value for PCF_r , P_{bot} and P_{top} as these process parameters can be found at the complete right
590 side of the loading plot, opposite from the PCD (blue dashed circle). The same rationale as
591 with main compression displacement can be followed to explain these observations.
592 Furthermore, the model shows the relation between the PCD and the variability of the process.
593 A cluster close to PCD on the loading plot with VC t_{dw} and VC T_{IDP} highlight that during
594 compression with displacement the variation in dwell time and in in-die thickness is larger than
595 in experiments where no displacement is used. Also here a cluster of VC $F_{mplateau}$, VC F_{max} and
596 VC AUC_{total} on the opposite site of the loading plot, reveal that the value of these variables is
597 lowered when displacement is used. From these observations can be concluded that also
598 during pre-compression with the moving roller set-up, the variability in the process is not
599 translated into variability in the force exerted on the powder bed, as is the case with the fixed
600 roller set-up.

601

602 Several other variables are positively or negatively correlated to PCD as seen on Figure 11
603 (blue dotted circles). Their position on the loading plot can be explained by the difference in
604 the shape of the force-time profile between compression with and without displacement
605 (Figure 6a and Figure 6c). Firstly, the position of the t/p_{mean} close to the PCD confirms that this
606 value is a suitable parameter to describe the shape of the force-time profile. Furthermore, for
607 the Y-axis of the force-time profile (force), the location of F_{max} and F_{bdw} for pre-compression
608 are logically, as these variables have a higher value when displacement is used. Since F_{75dw} ,
609 F_{min} and F_{edw} can be found on the opposite site of the plot, these variables are negatively
610 correlated with PCD, F_{max} and F_{bdw} . When comparing Figure 6a and Figure 6c, indeed can be
611 seen that these values are lower when displacement is used. F_{25dw} and F_{50dw} are not
612 significantly altered by compressing with or without displacement, which is supported by the

613 position of these variables in the loading plot, since they are located in the middle of the plot
614 according to PC3. For the X-axis of the force-time profile (time), the dwell time (t_{dw}) and related
615 values (t_{25dw} , t_{50dw} , t_{75dw} , t_{Fmin}) are increased. In contrast, t_{decomp} can be found at the right side
616 of the loading plot, so is negatively correlated with an increased displacement. From this can
617 be concluded that also during pre-compression the dwell time with the moving-roller is
618 prolonged.

619

620 When looking at the score of PC3 versus the scores of PC4 (Figure 10) along the Y-axis
621 (PC4), two clusters can be distinguished. Loadings for PC4 (Figure 11) show that experiments
622 with a lower score value (lower half of the score plot) were performed at a higher MCF (at the
623 bottom of the loading plot (red full line)) while experiments with higher PC4 scores (upper half
624 of the score plot) were performed at a lower MCF, which is also in accordance with the set-up
625 of the experiments (Figure 4). Closely correlated variables to the MCF (F_{max}) are clearly
626 clustered (F_{bdw} , F_{25dw} , F_{50dw} , F_{75dw} , $F_{mplateau}$, F_{edw} , F_{min}), as can be seen on the loading plot.
627 Moreover, experiments with a high score value according to PC4 have a high loading value
628 for T_{IDM} and $h_{BP(M)}$ as these process parameters can be found at the top of the loading plot,
629 opposite from the MCF (red dashed circle). This is expected, as the in-die thickness (T_{IDM}) and
630 distance between the punches (h_{BP}) is decreased when higher compression forces are used.

631

632 Based on the PCA-analysis, a few general conclusions can be drawn. Firstly, tableting speed
633 contributes to a large extent to the variance of PC1, the first PC in the model. This elucidates
634 how important tableting speed is in performing tableting experiments, as it contributes the
635 most to the observed variance. Mainly its influence on the shape of the force-time profile and
636 the dwell time has to be considered. Secondly, this analysis shows that the moving roller set-
637 up also influences to a great extent the tableting process

638 Moreover, the dimensionless parameter, t/p_{mean} ratio, can be considered a sensitive
639 parameter to describe the shape of the force-time profile within the range of the parameter
640 setting used. Finally, the main compression force contributes to a large extent to the variance

641 captured by PC4. Since PC4 only explains 9.8 % of the observed variance in the model, it can
642 be concluded that the tableting speed and the displacement have a larger influence on the
643 compression event (i.e. the other process variables) than the applied (main compression)
644 force.

645

646 **3.3.2. Partial Least Squares**

647

648 In order to examine the influence of the process parameters on the tablet properties, a PLS
649 model was constructed. PLS is a regression extension of PXA, which is used to connect the
650 information in two blocks of variables, X (the process parameters) and Y (the tablet properties)
651 [49]. In a first attempt to construct the model, all selected variation coefficients (VC) were
652 included in the model (see Table 3 and Table 4). However, a negative Q^2 value was obtained
653 for the first 2 PC's. This implies that the model has no predictive power when using only 2
654 PC's, and a third PC is necessary to force the model into cross validation predictions. Since
655 this approach has no rational basis, the model was adapted and all variation coefficients were
656 excluded. In this new model, three principal components (PCs) were fitted in the PLS model
657 explaining 66.8% (R^2) and predicting 18.1% (Q^2) of the variation in the data.

658

659 Scores of PC1 versus PC2 are depicted in Figure 12. Figure 13 is a plot of the loadings of
660 PC1 versus the loadings of PC2. Again, three clusters on the X-axis (PC1) are identifiable:
661 experiments on the left side were performed at a speed of 1000 tpm, on the center at a speed
662 of 500 tpm and on the right at a speed of 250 tpm. This is confirmed when looking at the
663 loading plot, where the variable speed is positioned on the left side of the plot (red full circle).
664 The loadings of the tablet properties located close to the variable speed are correlated with
665 this process parameter (red dashed circle). Mainly all the "Diff" variables, which depict the
666 difference between the mean value of the process parameter measured at t_0 and t_7 , are
667 related to the tableting speed. Since these variables have a high value, this means that the
668 values of these process parameters are higher after 1 week of storage, than measured

669 immediately after production. The observations can be explained by the viscoelastic behavior
670 of ibuprofen. IAR_{pre} and IAR_{main} have high values at high tableting speed. This means that the
671 immediate axial recovery (in-die) is higher at higher tableting speeds, as also reported in
672 literature [12, 20, 25, 27, 40, 50]. The axial recovery (relaxation) continuous further after
673 removal from the die and during storage (Diff (CAR-IAR)), as an increase in diameter (Diff D)
674 and thickness (Diff T) can be observed. Not only the dimensions of the tablet change, but also
675 an increase in tensile strength takes place, represented by Diff H, Diff TS and Hardening. This
676 suggest that the tablet not only expands slowly due to the viscoelastic nature of the material,
677 but that at the same time a reorganization of the material inside the tablet takes place,
678 contributing to a higher tensile strength. Although already reported in literature, a clear
679 explanation for this effect cannot be given [47]. Moreover, since the absolute values are small
680 (e.g. for thickness a maximum increase of 0.11 mm, diameter 0.03 mm and TS 0.16 MPa) this
681 dos not necessary imply any bio-relevant or critical qualitative changes.

682

683 When looking at the score of PC1 versus the scores of PC2 (Figure 12) along the Y-axis
684 (PC2), no clear clusters can be distinguished. Moreover, based on the experimental settings
685 (Figure 4) and the loadings for PC2 (Figure 13) it is clear that more than one process
686 parameter is contributing to the variance captured by PC2. The loading plot shows that
687 experiments with a lower score value (lower half of the score plot) were performed at a higher
688 MCD and a higher MCF (at the bottom of the loading plot (blue full circle)) while experiments
689 with higher PC2 scores (upper half of the score plot) were performed at a lower MCD and a
690 lower MCF. The loadings of the tablet properties close to these two process variables are the
691 hardness (H), TS and density (dens) of the tablets, both at t0 and t7 (blue dashed circle). The
692 correlation with a higher compression force is obvious, the contribution of the prolonged dwell
693 time (higher MCD) however as such cannot be determined. On the opposite site of the plot,
694 the tablet porosity (t0 and t7) can be found, as this parameter is the inverse of density.

695

696 Scores of PC2 versus PC3 are depicted in Figure 14. Figure 15 is a plot of the loadings of
697 PC2 versus the loadings of PC3. Although two clusters on the Y-axis (PC3) are identifiable, it
698 is clear that more than one process parameter is contributing to the variance captured by PC3.
699 The loading plot shows that experiments with a higher score value (upper half of the score
700 plot) were performed at a higher MCF and a higher PCF (at the left upper corner and top of
701 the loading plot (blue full circle)) while experiments with lower PC3 scores (lower right corner
702 and bottom of the score plot) were performed at a lower MCF and a lower PCF. The loading
703 of the tablet property close to the process variable PCF is the in- die density (dens ID (P))
704 (blue dashed circle). On the opposite site of the plot, the in-die porosity (por ID (P)) and in-die
705 volume (V ID (P)) can be found. The loadings of the tablet properties close to the process
706 variable MCF (blue dotted circle) are immediate axial recovery upon ejection (IAR t0) and the
707 axial recovery after storage (CAR). From this can be concluded that when tablets are
708 compressed at higher loads, the relaxation over time is prolonged. Moreover, based on these
709 observations it is clear that different process parameters have a different influence on the
710 relaxation behavior of material (i.e. the correlation between IAR_{pre} , IAR_{main} and tableting speed
711 and the correlation between IAR_{t0} , CAR with MCF) and that it is important to take all these
712 measurements into consideration. Other tablet properties related to a higher compression
713 force are the density, hardness and TS. On the opposite side of the plot, the porosity, volume
714 and thickness of the tablets are situated. It is interesting to note that the final tablet properties
715 are mainly determined by the final compression (i.e. main compression) step and not so much
716 by the pre-compression step, as the in-die properties at main compression (i.e. dens ID (M),
717 por ID (M), V ID (M) are closely related to the properties after ejection (and after storage) .
718 Since the process variable MCD is also located close to the loadings of the former tablet
719 properties (density, TS, H) it is possible that a higher MCD contributes to these tablet
720 characteristics, although clear conclusions cannot be drawn.

721

722 Overall, the PLS revealed that mainly the tableting speed and the main compression force
723 attribute to the final tablet properties. Furthermore, the relation between process parameters

724 and tablet properties is not straight forward, as the different variables all contribute
725 simultaneously to the final tablet characteristic and the variation captured by the different PC's
726 cannot be linked to one particular process variable. Although displacement seems to
727 contribute to (some of) the tablet characteristics, clear conclusions cannot be drawn. Finally,
728 a special reference should be made to the elastic behavior of ibuprofen. The PLS revealed
729 that a high compression speed and a high MCF both favor the elastic expansion (either in-die
730 or after ejection). This effect is known to increase the capping tendency of tablets. Although
731 not translated in the absolute values of hardness or friability, it should be mentioned that the
732 detrimental effect of higher elastic recovery at high speeds and high compression forces was
733 observed during friability and hardness testing. A large amount of tablets from experiment 3
734 and 5 at 1000 tpm (Figure 4) underwent capping upon radial pressure before breaking at the
735 hardness test after the storage period (33 and 50 % respectively). Also, during the friability
736 test, about half of these tablets broke into smaller pieces.

737

738 **3.4. Disintegration testing and SEM**

739

740 The data obtained from the disintegration test were not included in the PLS-analysis, as the
741 observed differences were not bio-relevant, with the shortest disintegration time being 102.57
742 ± 26.09 s and the longest 167.95 ± 18.06 s. A trend could be observed however, depending
743 on tableting speed and applied forces. The tableting speed had a negative influence on the
744 disintegration time, whereas an increase of the compression force increased the time the
745 tablets needed to disintegrate.

746

747 SEM-pictures were taken from the tablet surfaces (not shown). Overall, it could be concluded
748 that the surfaces of the tablets were similar, although an influence of the tableting speed and
749 the compression force could also here be observed. In those experiments where lower
750 tableting speeds and higher compression forces were used, a slightly smoother surface was
751 obtained. The difference becomes more pronounced when comparing the experiments (of

752 each tableting speed) who were performed with and without displacement (extended dwell
753 time), and this both on pre- and main compression. The tablets produced with displacement
754 had markedly smoother surfaces than the tablets produced without. This observation might
755 explain partly the lower ejection forces obtained with displacement at main compression, as
756 could be concluded from the PCA-analysis. Smoother surfaces will adhere less to the punch
757 tips and die-wall, reducing the force necessary to overcome this adherence and consequently
758 lowering the ejection force.

759

760 **4. Conclusions**

761

762 Principal Component Analysis (PCA) provided an overview of the main underlying phenomena
763 in the performed tableting experiments. The main source of variation in this dataset was
764 captured in PC1 which is composed mainly by the changes caused by an alteration of the
765 tableting speed. The second major direction of variation in the dataset (PC2) is the change in
766 main compression displacement. PC3 is mainly composed by the displacement at pre-
767 compression and correlated variables. At last, the main compression force contributes to a
768 large extent to the variance captured by PC4. Partial Least Squares (PLS) revealed that mainly
769 the tableting speed and the main compression force attribute to the final tablet properties and
770 that the relation between process parameters and tablet properties is not straight forward, as
771 the different variables all contribute simultaneously to the final tablet characteristics. Overall,
772 this analysis provided a summary of the contribution of the moving roller set-up to the tableting
773 process and tablet properties. This research project shows that a large amount of parameters
774 influence the compression cycle and it is difficult, if not impossible, to study the contribution of
775 all factors separately. Using an instrumented high speed rotary press, a large amount of
776 information is obtained which contributes to the further understanding of this complex
777 engineering process.

778

779 **Acknowledgements**

780

781 Authors would like to thank Sanico (Turnhout, Belgium) for their kind donation of the granules.
782 Dr. Ir. Frederik Detobel and Benny Van der Steen from GEA Process Engineering (Halle,
783 Belgium) are gratefully acknowledged for the fruitful discussions and their technical support in
784 this work.

785

786 **Data Statement**

787

788 Primary raw data could not be provided as they are only available in a format readable by the
789 customized software application (CDAAS). The data table (20 rows, 169 columns) which was
790 used for the multivariate data analysis was made electronically available. It contains all
791 calculated mean values and variation coefficients of the machine settings, the data logged by
792 the tablet press and the CDAAS software and the tablet properties [48].

793

794 **Declarations of Interest**

795

796 None.

797

798 **References**

799

800 [1] C. De Brabander, C. Vervaet, L. Van Bortel, J.P. Remon, Bioavailability of ibuprofen from
801 hot-melt extruded mini-matrices, *Int. J. Pharm.* 271 (2004) 77-84. doi:
802 [10.1016/j.ijpharm.2003.10.029](https://doi.org/10.1016/j.ijpharm.2003.10.029)

803 [2] P.V. Marshall, P. York, J.Q. Maclaine, An investigation of the effect of the punch velocity
804 on the compaction properties of ibuprofen, *Powder Technol.* 73 (1993) 171-177. doi:
805 [10.1016/0032-5910\(93\)87009-D](https://doi.org/10.1016/0032-5910(93)87009-D)

806 [3] N. Rasenack, B.W. Müller, Crystal habit and tableting behavior, *Int. J. Pharm.* 244 (2002)
807 45-57. doi: [10.1016/S0378-5173\(02\)00296-X](https://doi.org/10.1016/S0378-5173(02)00296-X)

- 808 [4] N.F. Abu Bakar, A. Mujumdar, S. Urabe, K. Takano, K. Nishii, M. Horio, Improvement of
809 sticking tendency of granules during tableting process by pressure swing granulation, Powder
810 Technol. 176 (2007) 137-147. doi: [10.1016/j.powtec.2007.02.037](https://doi.org/10.1016/j.powtec.2007.02.037)
- 811 [5] K. Kachrimanis, G. Kistis, S. Malamataris, Crystallisation conditions and
812 physicochemical properties of ibuprofen-Eudragit® S100 spherical crystal agglomerates
813 prepared by the solvent-change technique, Int. J. Pharm. 173 (1998) 61-74. doi:
814 [10.1016/S0378-5173\(98\)00191-4](https://doi.org/10.1016/S0378-5173(98)00191-4)
- 815 [6] P. Di Martino, M. Beccerica, E. Joiris, G.F. Palmieri, A. Gayot, S. Martelli, Influence of
816 chystal habit on the compression and densification mechanism of ibuprofen, J. Cryst. Growth
817 243 (2002) 345-355. doi: [10.1016/S0022-0248\(02\)01523-3](https://doi.org/10.1016/S0022-0248(02)01523-3)
- 818 [7] H.A. Garekani, D. Sadeghi, A. Badiiee, S.A. Mostafa, A.R. Rajabi-Siahboomi, Crystal habit
819 modifications of ibuprofen and their physicochemical characteristics, Drug Dev. Ind. Pharm.
820 27 (2001) 803-809. doi: [10.1081/DDC-100107243](https://doi.org/10.1081/DDC-100107243)
- 821 [8] P.K. More, K.S. Khomane, A.K. Bansal, Flow and compaction behaviour of ultrafine coated
822 ibuprofen, Int. J. Pharm. 441 (2013) 527-534. doi: [10.1016/j.ijpharm.2012.10.048](https://doi.org/10.1016/j.ijpharm.2012.10.048)
- 823 [9] S. Patel, A.M. Kaushal, A.K. Bansal, Compaction behavior of roller compacted ibuprofen,
824 Eur. J. Pharm. Biopharm. 69 (2008) 743-749. doi: [10.1016/j.ejpb.2008.01.005](https://doi.org/10.1016/j.ejpb.2008.01.005)
- 825 [10] N. Rasenack, B.W. Müller, Ibuprofen crystal with optimized properties, Int. J. Pharm. 245
826 (2002) 9-24. doi: [10.1016/S0378-5173\(02\)00294-6](https://doi.org/10.1016/S0378-5173(02)00294-6)
- 827 [11] L. Seton, M. Roberts, F. Ur-Rehman, Compaction of recrystallised ibuprofen, Chem. Eng.
828 J. 164 (2010) 449-452. doi: [10.1016/j.cej.2009.10.037](https://doi.org/10.1016/j.cej.2009.10.037)
- 829 [12] A. Nokhodchi, M.H. Rubinstein, H. Larhrib, J.C. Guyot, The effect of moisture on the
830 properties of ibuprofen tablets, Int. J. Pharm. 118 (1995) 191-197. doi: [10.1016/0378-
831 5173\(94\)00354-8](https://doi.org/10.1016/0378-5173(94)00354-8)
- 832 [13] A. Nokhodchi, M.H. Rubinstein, H. Larhrib, J.C. Guyot, The effect of moisture content on
833 the energies involved in the compaction of ibuprofen, Int. J. Pharm. 120 (1995) 13-20. doi:
834 [10.1016/0378-5173\(94\)00372-C](https://doi.org/10.1016/0378-5173(94)00372-C)
- 835 [14] M. Roberts, J.L. Ford, G.S. MacLeod, J.T. Fell, G.W. Smith, P.H. Rowe, Effects of surface
836 roughness and chrome plating of punch tips on the sticking tendencies of model ibuprofen
837 formulations, J. Pharm. Pharmacol. 55 (2003) 1223-1228. doi: [10.1211/0022357021684](https://doi.org/10.1211/0022357021684)

- 838 [15] M. Roberts, J.L. Ford, G.S. MacLeod, J.T. Fell, G.W. Smith, P.H. Rowe, A.M. Dyas,
839 Effects of punch tip geometry and embossment on the punch tip adherence of a model
840 ibuprofen formulation, *J. Pharm. Pharmacol.* 56 (2004) 947-950. doi: [10.1211/0022357023736](https://doi.org/10.1211/0022357023736)
- 841 [16] M. Leitritz, M. Krumme, P.C. Schmidt, Force-time curves of a rotary tablet press.
842 Interpretation of the compressibility of a modified starch containing various amounts of
843 moisture, *J. Pharm. Pharmacol.* 48 (1996) 456-462. doi: [10.1111/j.2042-7158.1996.tb05954.x](https://doi.org/10.1111/j.2042-7158.1996.tb05954.x)
- 844 [17] J. Van Evelghem, Improving tablet quality with compression to equal force technology,
845 *Pharm. Tech. (Suppl.)* 32 (2008) 26-29.
- 846 [18] R.L. Carr, Evaluating flow properties of solids, *Chem. Eng.* 72 (1965) 163-168.
- 847 [19] M. J. Bogda, Tablet compression: Machine theory, design, and process troubleshooting,
848 in: J. Swarbrick (Ed.), *Encyclopedia of pharmaceutical technology* Informa Healthcare USA
849 Inc., New York, 2007, pp.3611-3629.
- 850 [20] O. F. Akande, J.L. Ford, P.H. Rowe, M.H. Rubinstein, The effects of lag-time and dwell-
851 time on the compaction properties of 1:1 paracetamol/microcrystalline cellulose tablets
852 prepared by pre-compression and main compression, *J. Pharm. Pharmacol.* 50 (1998) 19-28.
853 doi: [10.1111/j.2042-7158.1998.tb03300.x](https://doi.org/10.1111/j.2042-7158.1998.tb03300.x)
- 854 [21] C.E. Ruegger, M. Celik, The influence of varying precompaction and main compaction
855 profile parameters on the mechanical strength of compacts, *Pharm. Dev. Technol.* 5 (2000) 495-
856 505. doi: [10.1081/PDT-100102033](https://doi.org/10.1081/PDT-100102033)
- 857 [22] I.C. Sinka, F. Motazedian, A.C.F. Cocks, K.G. Pitt, The effect of processing parameters
858 on pharmaceutical tablet properties, *Powder Technol.* 189 (2009) 276-284. doi:
859 [10.1016/j.powtec.2008.04.020](https://doi.org/10.1016/j.powtec.2008.04.020)
- 860 [23] E.N. Hiestand, J.E. Wells, C.B. Peot, J.E. Ochs, Physical processes in tableting, *J. Pharm.*
861 *Sci.* 66 (1977) 510-519. doi: [10.1002/jps.2600660413](https://doi.org/10.1002/jps.2600660413)
- 862 [24] N.A. Armstrong, Tablet manufacture, in: J. Swarbrick (Ed.), *Encyclopedia of*
863 *pharmaceutical technology* Informa Healthcare USA Inc., New York, 2007, pp.3653-3672.
- 864 [25] R.V. Haware, I. Tho, A. Bauer-Brandl, Evaluation of a rapid approximation method for the
865 elastic recovery of tablets, *Powder Technol.* 202 (2010) 71-77. doi:
866 [10.1016/j.powtec.2010.04.012](https://doi.org/10.1016/j.powtec.2010.04.012)

- 867 [26] T.M. Jones, The physicochemical properties of starting materials used in tablet
868 formulation, *Int. J. Pharm. Tech. Prod. Manuf.* 2 (1981) 17-24.
- 869 [27] P. Konkel, J.B. Mielck, Associations of parameters characterizing the time course of the
870 tableting process on a reciprocating and on a rotary tableting machine for high-speed
871 production, *Eur. J. Pharm. Sci.* 45 (1998) 137-148. doi: [10.1016/S0939-6411\(98\)00020-4](https://doi.org/10.1016/S0939-6411(98)00020-4)
- 872 [28] M. Levin, Tablet press instrumentation, in: J. Swarbrick (Ed.), *Encyclopedia of*
873 *pharmaceutical technology* Informa Healthcare USA Inc., New York, 2007, pp.3684-3706.
- 874 [29] A. Munoz Ruiz, M.R. Jimenez-Castellanos, J.C. Cunningham, A.V. Katdare, Theoretical
875 estimation of dwell and consolidation times in rotary tablet machines, *Drug Dev. Ind. Pharm.*
876 18 (1992) 2011-2028. doi: [10.3109/03639049209040917](https://doi.org/10.3109/03639049209040917)
- 877 [30] A.S. Narang, V.M. Rao, H. Guo, J.A. Lu, D.S. Desai, Effect of force feeder on tablet
878 strength during compression, *Int. J. Pharm.* 401 (2010) 7-15. doi:
879 [10.1016/j.ijpharm.2010.08.027](https://doi.org/10.1016/j.ijpharm.2010.08.027)
- 880 [31] C.E. Ruegger, M. Celik, The effect of compression and decompression speed on the
881 mechanical strength of compacts, *Pharm. Dev. Technol.* 5 (2000) 485-494. doi: [10.1081/PDT-](https://doi.org/10.1081/PDT-100102032)
882 [100102032](https://doi.org/10.1081/PDT-100102032)
- 883 [32] C.E. Rowlings, A.Y. Leung, P.C. Sheen, Resolution of the material and machine
884 contributions to the area to height ratio obtained from force-time powder compression data II:
885 Rotary tablet press, *Pharm. Acta Helv.* 72 (1997) 125-130. doi: [10.1016/S0031-](https://doi.org/10.1016/S0031-6865(97)00008-3)
886 [6865\(97\)00008-3](https://doi.org/10.1016/S0031-6865(97)00008-3)
- 887 [33] P.C. Schmidt, P.J. Vogel, Force-time-curves of a modern rotary tablet machine I.
888 Evaluation techniques and characterization of deformation behaviour of pharmaceutical
889 substances, *Drug Dev. Ind. Pharm.* 20 (1994) 921-934. doi: [10.3109/03639049409038341](https://doi.org/10.3109/03639049409038341)
- 890 [34] P.C. Schmidt, M. Leitritz, Compression force/time-profiles of microcrystalline cellulose,
891 dicalcium phosphate dihydrate and their binary mixtures – a critical consideration of
892 experimental parameters, *Eur. J. Pharm. Biopharm.* 44 (1997) 303-313. doi: [10.1016/S0939-](https://doi.org/10.1016/S0939-6411(97)00129-X)
893 [6411\(97\)00129-X](https://doi.org/10.1016/S0939-6411(97)00129-X)
- 894 [35] C.K. Tye, C. Sun, G.E. Amidon, Evaluation of the effects of tableting speed on the
895 relationships between compaction pressure, tablet tensile strength, and tablet solid fraction,
896 *J. Pharm. Sci.* 94 (2005) 465-472. doi: [10.1002/jps.20262](https://doi.org/10.1002/jps.20262)

897 [36] P.J. Vogel, P.C. Schmidt, Force-time curves of a modern rotary tablet machine II.
898 Influence of compression force and tableting speed on the deformation mechanisms of
899 pharmaceutical substances, *Drug Dev. Ind. Pharm.* 19 (1993) 1917-1930. doi:
900 [10.3109/03639049309073898](https://doi.org/10.3109/03639049309073898)

901 [37] J.K. Yliruusi, O.K. Antikainen, New parameters derived from tablet compression curves.
902 Part I. Force-Time curve, *Drug Dev. Ind. Pharm.* 23 (1997) 69-79. doi:
903 [10.3109/03639049709148483](https://doi.org/10.3109/03639049709148483)

904 [38] C. Sun, D.J.W. Grant, Influence of crystal structure on the tableting properties of
905 sulfamerazine polymorphs, *Pharm. Res.* 18 (2001) 274-280. doi: [10.1023/A:1011038526805](https://doi.org/10.1023/A:1011038526805)

906 [39] C. Sun, M.W. Himmelspach, Reduced tableability of roller compacted granules as a result
907 of granule size enlargement, *J. Pharm. Sci.* 95 (2006) 200-206. doi: [10.1002/jps.20531](https://doi.org/10.1002/jps.20531)

908 [40] S.L. Cantor, S.W. Hoag, L.L. Augsburger, Evaluation of the mechanical properties of
909 extrusion-spheronized beads and multiparticulate systems, *Drug Dev. Ind. Pharm.* 35 (2009)
910 683-693. doi: [10.1080/03639040802526797](https://doi.org/10.1080/03639040802526797)

911 [41] E. Joiris, P. Di Martino, C. Berneron, A.M. Guyot-Hermann, J.C. Guyot, Compression
912 behavior of orthorhombic paracetamol, *Pharm. Res.* 15 (1998) 1122-1130. doi:
913 [10.1023/A:1011954800246](https://doi.org/10.1023/A:1011954800246)

914 [42] E. Peeters, T. De Beer, C. Vervaet, J.P. Remon, Reduction of tablet weight variability by
915 optimizing paddle speed in the forced feeder of a high-speed rotary tablet press, *Drug Dev.*
916 *Ind. Pharm.* 41 (2015) 530-539. doi: [10.3109/03639045.2014.884121](https://doi.org/10.3109/03639045.2014.884121)

917 [43] D. Natoli, M. Levin, L. Tsygan, L. Liu, Development, optimization, and scale-up of process
918 parameters: Tablet compression, in: Y. Qiu, Y. Chen, G.G.Z. Zhang, L. Liu, W.R. Porter (Eds.),
919 *Developing Solid Oral Dosage Forms, Pharmaceutical Theory and Practice*, Elsevier Inc., New
920 York, 2009, pp. 725-759.

921 [44] J.T. Fell, J.M. Newton, Determination of Tablet Strength by Diametral-Compression Test,
922 *J. Pharm. Sci.* 59 (1970) 688-691. doi: [10.1002/jps.2600590523](https://doi.org/10.1002/jps.2600590523)

923 [45] N.A. Armstrong, R.F. Haines-Nutt, Elastic recovery and surface area changes in
924 compacted powder systems, *J. Pharm. Pharmacol.* 24 (1972) 135P-136P. doi: [10.1016/0032-
925 5910\(74\)80054-9](https://doi.org/10.1016/0032-5910(74)80054-9)

- 926 [46] A. Adolfsson, C. Nystrom, Tablet strength, porosity, elasticity and solid state structure of
927 tablets compressed at high loads, *Int. J. Pharm.* 132 (1996) 95-106. doi: [10.1016/0378-
928 5173\(95\)04336-5](https://doi.org/10.1016/0378-5173(95)04336-5)
- 929 [47] K.M. Picker, Time dependence of elastic recovery for characterization of tableting
930 materials, *Pharm. Dev. Technol.* 6 (2001) 61-70. doi: [10.1081/PDT-100000014](https://doi.org/10.1081/PDT-100000014)
- 931 [dataset] [48] E. Peeters, A.F.T. Silva, M. Fonteyne, T. De Beer, C. Vervaet, J.P. Remon, Data
932 Table of Influence of extended dwell time during pre- and main compression on the properties
933 of ibuprofen, *Mendeley Data*, v1, 2018. <http://dx.doi.org/10.17632/drwddcpyn7.1>
- 934 [49] L. Eriksson, E. Johansson, N. Kettaneh-Wold, J. Trygg, C. Wikström, S. Wold, Multi- and
935 Megavariate data analysis, part I, basic principles and applications, second ed., Umetrics,
936 Umea, 2006.
- 937 [50] R.J. Roberts, R.C. Rowe, The effect of punch velocity on the compaction of a variety of
938 materials, *J. Pharm. Pharmacol.* 37 (1985) 377-384. doi: 10.1111/j.2042-7158.1985.tb03019.x

939 **Tables**

940

941 Table 1: Initial set-up of the experimental design.

942

943 Table 2: Overview of the machine settings. The settings included in the PCA and PLS-analysis
944 are marked with ♦.

945

946 Table 3: Overview of parameters derived from the logged data. The settings included in the
947 PCA and PLS-analysis are marked: ♦ if only the absolute value was taken into account, ♦♦ if
948 also the variation coefficient (VC) was included in the data.

949

950 Table 4: Overview of the tablet characteristics. The settings included in the PLS-analysis are
951 marked: ♦ if only the absolute value was taken into account, ♦♦ if also the variation coefficient
952 (VC) was included in the data.

953

954 Table 5: Flow properties, true density and particle size distribution of the granules.

955 Table 1: Initial set-up of the experimental design.

Process variable	Lower level	Mid level	Upper level
Tableting speed (tpm)	250	500	1000
Precompression displacement (mm)	0	-	1
Main compression displacement (mm)	0	-	1

956 Table 2: Overview of the machine settings. The settings included in the PCA and PLS-analysis
 957 are marked with ◆.

Key	Meaning	Incl.
speed (tpm)	Tableting speed	◆
pad1 (rpm)	Speed of paddle 1 in the forced feeder	
pad2 (rpm)	Speed of paddle 2 in the forced feeder	
fill (mm)	Fill depth, which determines the weight	◆
CF _r (kN) ^a	Air pressure in the air-compensator above the top roller	◆
bot (mm) ^a	Position of bottom roller	◆
top (mm) ^a	Position of top roller	◆

958 ^a Different values for pre- (P) and main (M) compression.

959 Table 3: Overview of parameters derived from the logged data. The settings included in the
 960 PCA and PLS-analysis are marked: ♦ if only the absolute value was taken into account, ♦♦ if
 961 also the variation coefficient (VC) was included in the data.

Key	Meaning	Incl.
Force-Time profile ^a		
AUC _{total} (kN*ms)	Area under the curve of the complete profile	♦♦
t _{total} (ms)	Contact time	♦♦
AUC _{con} (kN*ms)	Area under the curve of the consolidation phase	♦
t _{con} (ms)	Consolidation time	♦
S _{con}	Slope of the consolidation phase	♦
AUC _{decomp}	Area under the curve of the decompression phase	♦
t _{decomp} (ms)	Decompression time	♦
S _{decomp}	Slope of the decompression phase	♦
t _{dw} (ms)	Dwell time	♦♦
F _{bdw} (kN)	Force at the beginning of the dwell time	♦
F _{edw} (kN)	Force at the end of the dwell time	♦
t _{25dw} (ms)	First quarter of the dwell time	♦
F _{25dw} (kN)	Force at 25% of the dwell time	♦
t _{50dw} (ms)	Middle of the dwell time	♦
F _{50dw} (kN)	Force at 50% of the dwell time	♦
t _{75dw} (ms)	Third quarter of the dwell time	♦
F _{75dw} (kN)	Force at 75% of the dwell time	♦
t _{Fmax} (ms)	Time when maximum force occurs	♦♦
F _{max} (kN)	Maximum force	♦♦
t _{Fmin} (ms)	Time when minimum force occurs	♦
F _{min} (kN)	Minimum force	♦
F _{mplateau} (kN)	Mean force of F _{25dw} , F _{50dw} , F _{75dw}	♦♦
t/p _{mean}	Ratio of F _{max} to F _{mplateau}	♦
Ejection profile		
F _{ejec} (kN)	Maximum ejection force	♦
Displacement-time profiles ^a		
CD (mm)	Maximum displacement of the upper roller	♦
Punch strokes		
h _{BT} (mm) ^a	Minimum distance between upper and lower punch during compression	♦
T _{ID} (mm) ^a	Minimum in-die thickness during compression	♦♦
T _{AD} (mm) ^a	In-die thickness immediately after the decompression phase	♦
t _{lag} (ms)	The time between pre- and main compression, measured on lower roller	♦

962 ^a Different values for pre- (P) and main (M) compression.

963 Table 4: Overview of the tablet characteristics. The settings included in the PLS-analysis are
 964 marked: ♦ if only the absolute value was taken into account, ♦♦ if also the variation coefficient
 965 (VC) was included in the data.

Key	Meaning	Incl.
W (mg) ^a	Tablet weight	♦
T (mm) ^a	Tablet thickness	♦♦
D (mm) ^a	Tablet diameter	♦
H (N) ^a	Hardness	♦
TS (MPa) ^a	Tensile strength	♦♦
Fria (%)	Friability	♦
Disint (s)	Disintegration	
V _{ID} ^b	Volume of the tablets during compressing, with minimum distance between punches	♦
V ^a	Volume of the tablets after ejection	♦
ρ _{ID} ^b	Density of the tablets during compressing, with minimum distance between punches	♦
P ^a	Density of the tablets after ejection	♦
ε _{ID} ^b	Porosity of the tablets during compressing, with minimum distance between punches	♦♦
E ^a	Porosity of the tablets after ejection	♦♦
IAR _{pre} (%)	Immediate axial recovery after the decompression phase at pre-compression	♦
IAR _{main} (%)	Immediate axial recovery after the decompression phase at main compression	♦
IAR _{t0} (%)	Immediate axial recovery of the tablets after ejection from the die	♦
CAR (%)	Cumulative axial recovery of the tablets after a storage period of 7 days	♦
Hardening (%)	Change in TS of the tablets upon storage	♦
Diff (CAR-IAR)	Difference between the IAR _{t0} and CAR	♦
Diff W (mg)	Difference in weight between t0 and t7	♦
Diff T (mm)	Difference in thickness between t0 and t7	♦
Diff D (mm)	Difference in diameter between t0 and t7	♦
Diff H (N)	Difference in hardness between t0 and t7	♦
Diff TS (MPa)	Difference in tensile strength between t0 and t7	♦

966 ^a Different values for measurements immediately after ejection (t0) and after the storage period
 967 (t7).

968 ^b Different values for pre- (P) and main (M) compression.

969 Table 5: Flow properties, true density and particle size distribution of the granules.

$\rho_{\text{bulk}}(\text{g}/\text{cm}^3)$	$\rho_{\text{tapped}}(\text{g}/\text{cm}^3)$	CI (%)	$\rho_{\text{true}}(\text{g}/\text{cm}^3)$	Particle size distribution		
				d10 (μm)	d50 (μm)	d90 (μm)
0.56 ± 0.00	0.67 ± 0.01	17.34 ± 0.59	1.24 ± 0.00	11.6 ± 0.6	66.2 ± 0.8	527.3 ± 3.5

970

971 **Figures**

972

973 Figure 1: Schematic representation of the pneumatic air compensator.

974

975 Figure 2: Schematic overview of the different positions and movements of rollers and punches
976 (a) with fixed rollers and (b) with moving rollers, highlighted by red lines and arrows. -·-·-
977 depicts the punch movement of the upper punch, --- depicts the movement of the lower
978 punch.

979

980 Figure 3: Representative illustration of theoretical (I) and observed (II) compression profile for
981 tablets compressed without (a) and with (b) displacement.

982

983 Figure 4: Schematic overview of the performed experiments. Red bars indicate the initial force
984 (2 kN at pre-compression, 12 kN at main compression).

985

986 Figure 5: Example of the data-logging. X-axis represent time (ms), left Y-axis represent
987 distance (mm), right Y-axis represents force (kN). Offset on Y-axis is intentionally changed to
988 permit better visibility of different values.

989

990 Figure 6: Schematic overview of the parameters determined from the force-time profiles for
991 tablets compressed without displacement at main compression (a) and pre-compression (b)
992 and with displacement (c) (both at pre- and main compression).

993

994 Figure 7: Plot representing the tabletability. Tensile strength (TS) is plotted against main
995 compression force (MCF).

996

997 Figure 8: Score scatter plot of PC1 vs. PC 2. [t1] Scores of Principal Component 1; [t2] Scores
998 of Principal Component 2.

999

1000 Figure 9: Loading scatter plot of PC1 vs. PC 2. [p1] Scores of Principal Component 1; [p2]
1001 Scores of Principal Component 2. Key: see Table 2 and Table 3.

1002

1003 Figure 10: Score scatter plot of PC3 vs. PC 4. [t3] Scores of Principal Component 3; [t4] Scores
1004 of Principal Component 4.

1005

1006 Figure 11: Loading scatter plot of PC3 vs. PC 4. [p3] Loadings of Principal Component 3; [p4]
1007 Loadings of Principal Component 4. Key: see Table 2 and Table 3.

1008

1009 Figure 12: Score scatter plot of PC1 vs. PC 2. [t1] Scores of Principal Component 1; [t2] Scores
1010 of Principal Component 2.

1011

1012 Figure 13: Loading scatter plot of PC1 vs. PC 2. w*c[1] Loadings of Principal Component 1;
1013 w*c[2] Loadings of Principal Component 2. Key: see Table 2, Table 3 and Table 4.

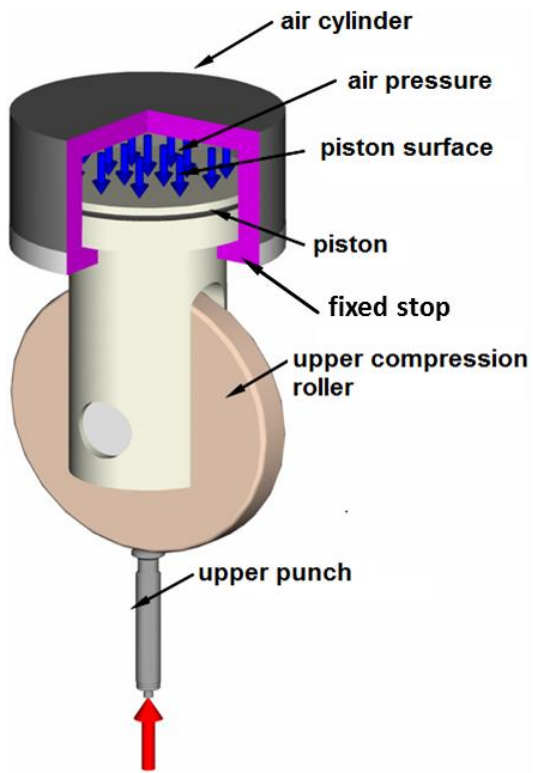
1014

1015 Figure 14: Score scatter plot of PC2 vs. PC 3. [t2] Scores of Principal Component 2; [t3] Scores
1016 of Principal Component 3.

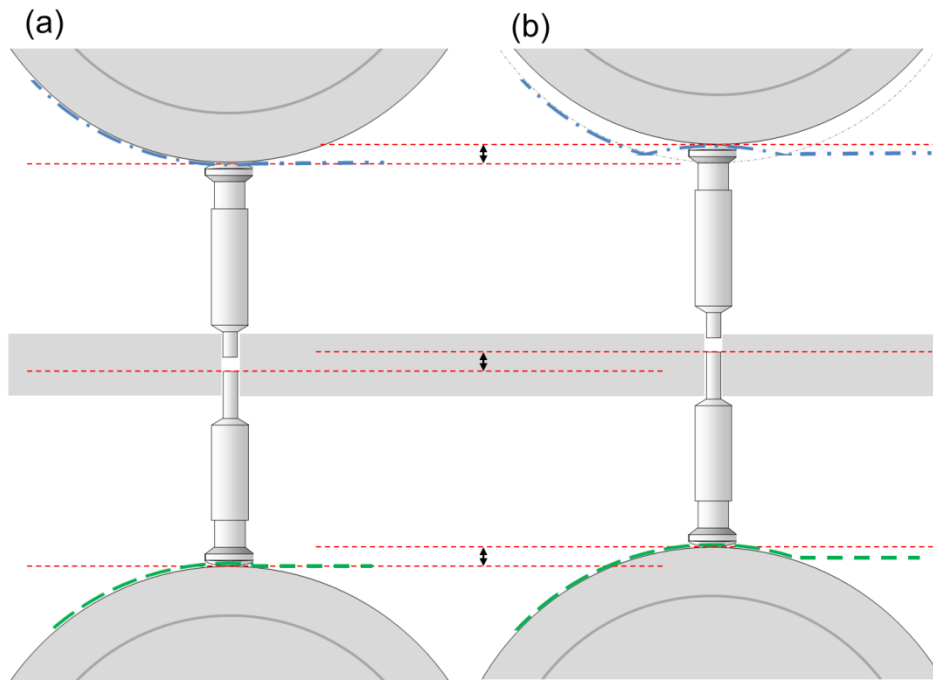
1017

1018 Figure 15: Loading scatter plot of PC2 vs. PC 3. w*c[2] Loadings of Principal Component 2;
1019 w*c[3] Loadings of Principal Component 3. Key: see Table 2, Table 3 and Table 4.

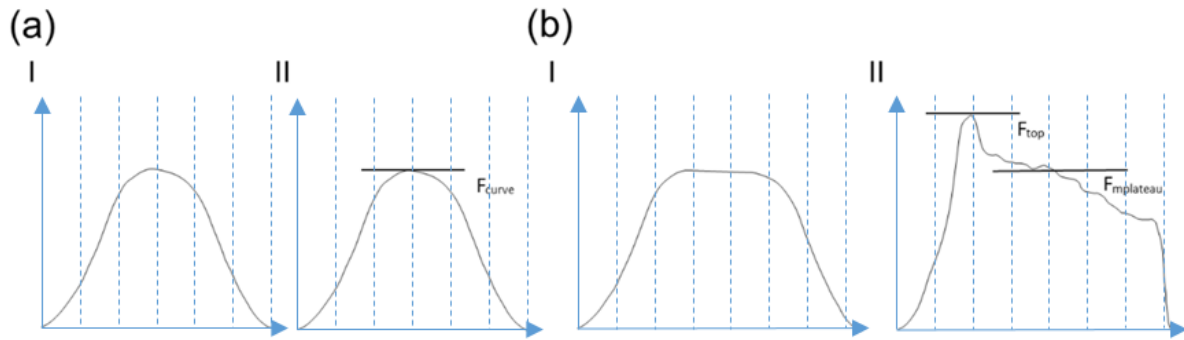
1020 Figure 1: Schematic representation of the pneumatic air compressor.



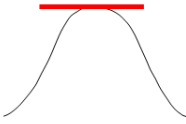
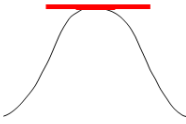
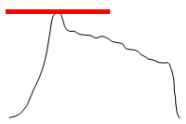
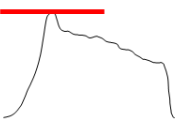
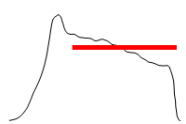
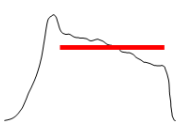
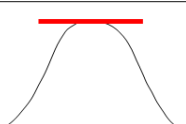
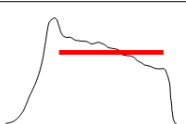
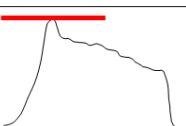
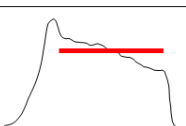
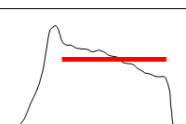
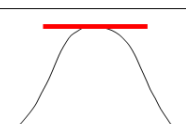
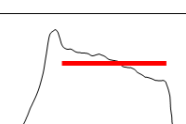
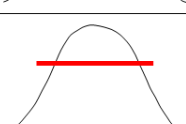
1021 Figure 2: Schematic overview of the different positions and movements of rollers and punches
1022 (a) with fixed rollers and (b) with moving rollers, highlighted by red lines and arrows. -·-·
1023 depicts the punch movement of the upper punch, --- depicts the movement of the lower
1024 punch.



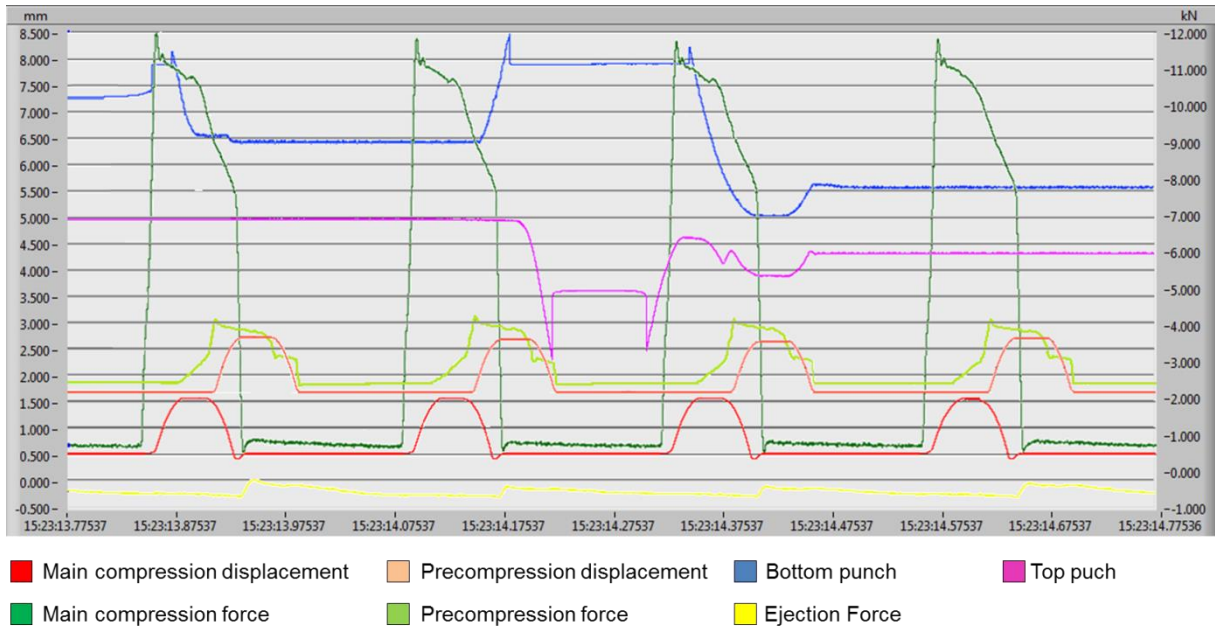
1025 Figure 3: Representative illustration of theoretical (I) and observed (II) compression profile for
1026 tablets compressed without (a) and with (b) displacement.



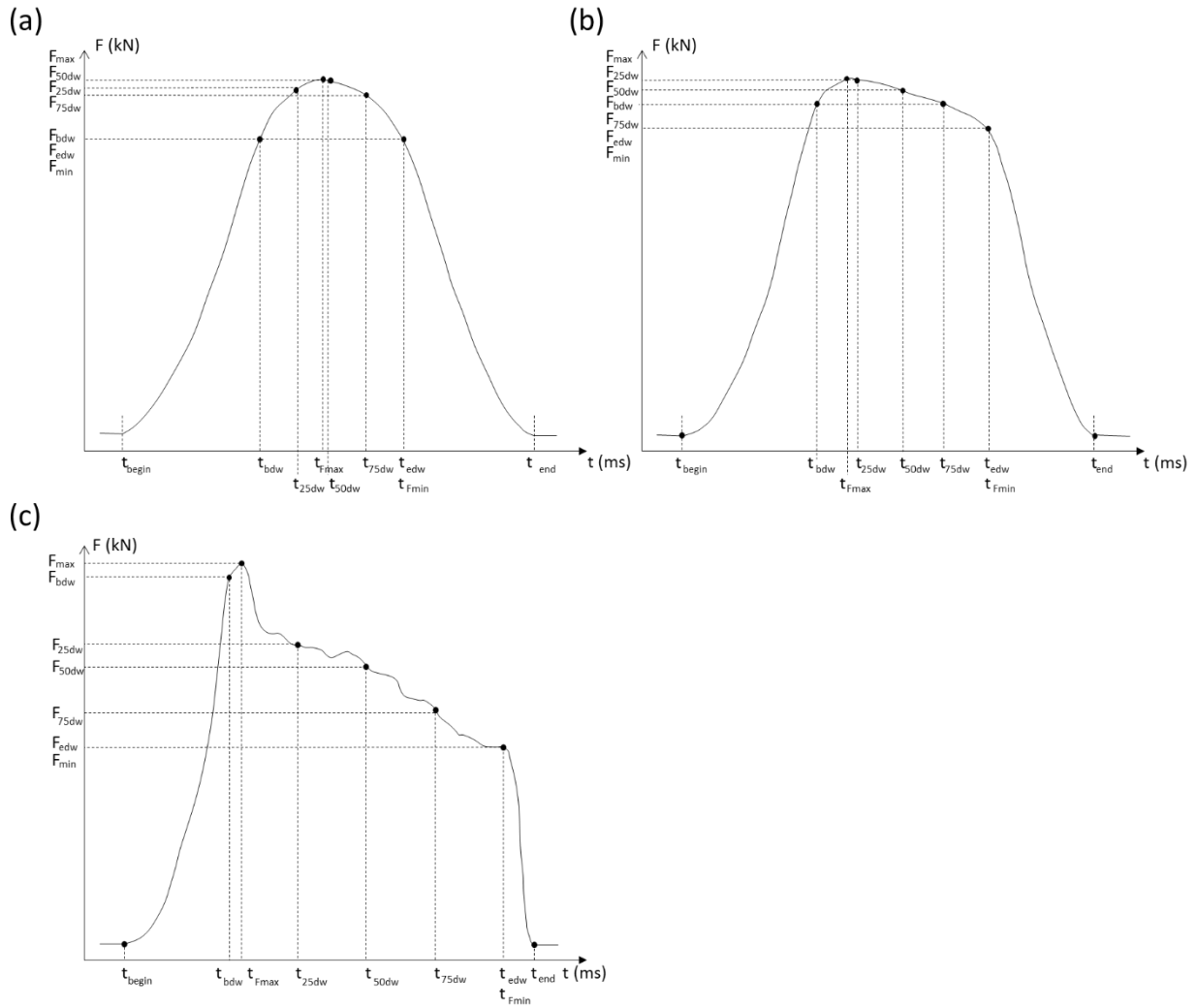
1027 Figure 4: Schematic overview of the performed experiments. Red bars indicate the initial force
 1028 (2 kN at pre-compression, 12 kN at main compression).

Experiment	Speed (rpm)		Precompression		Main compression	
	250	500	Shape	Displacement	Shape	Displacement
1	8	15		no		no
2	9	16		yes		yes
3	10	17		yes		yes
4	11	18		no		yes
5	12	19		yes		yes
6	13	20		yes		no
7	14	21		yes		no

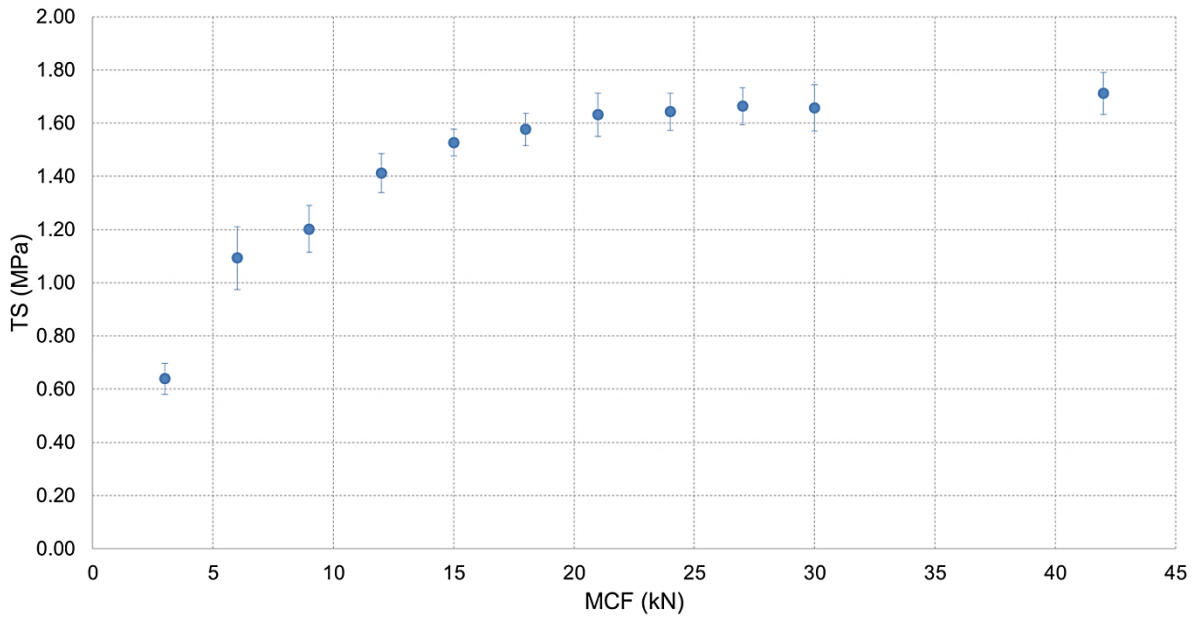
1029 Figure 5: Example of the data-logging. X-axis represent time (ms), left Y-axis represent
1030 distance (mm), right Y-axis represents force (kN). Offset on Y-axis is intentionally changed to
1031 permit better visibility of different values.



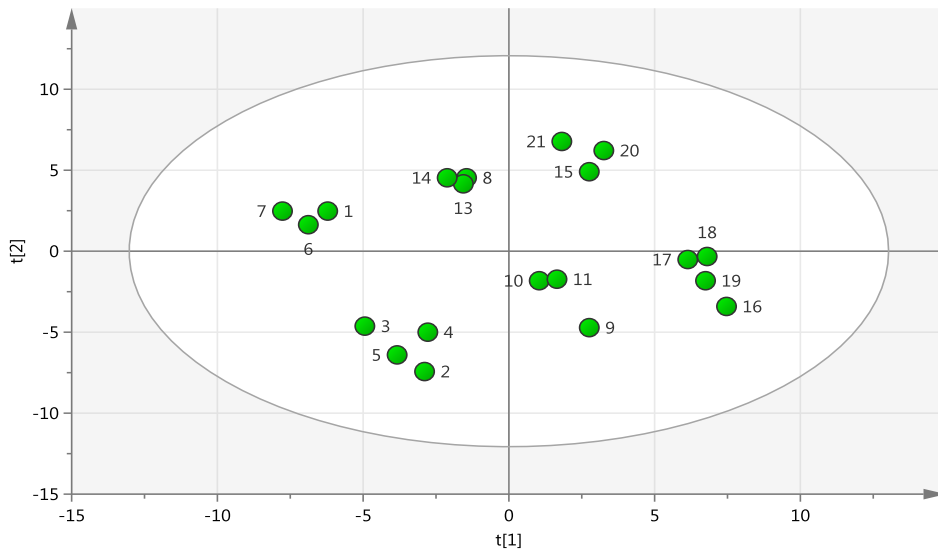
1032 Figure 6: Schematic overview of the parameters determined from the force-time profiles for
 1033 tablets compressed without displacement at main compression (a) and pre-compression (b)
 1034 and with displacement (c) (both at pre- and main compression).



1035 Figure 7: Plot representing the tableability. Tensile strength (TS) is plotted against main
1036 compression force (MCF).

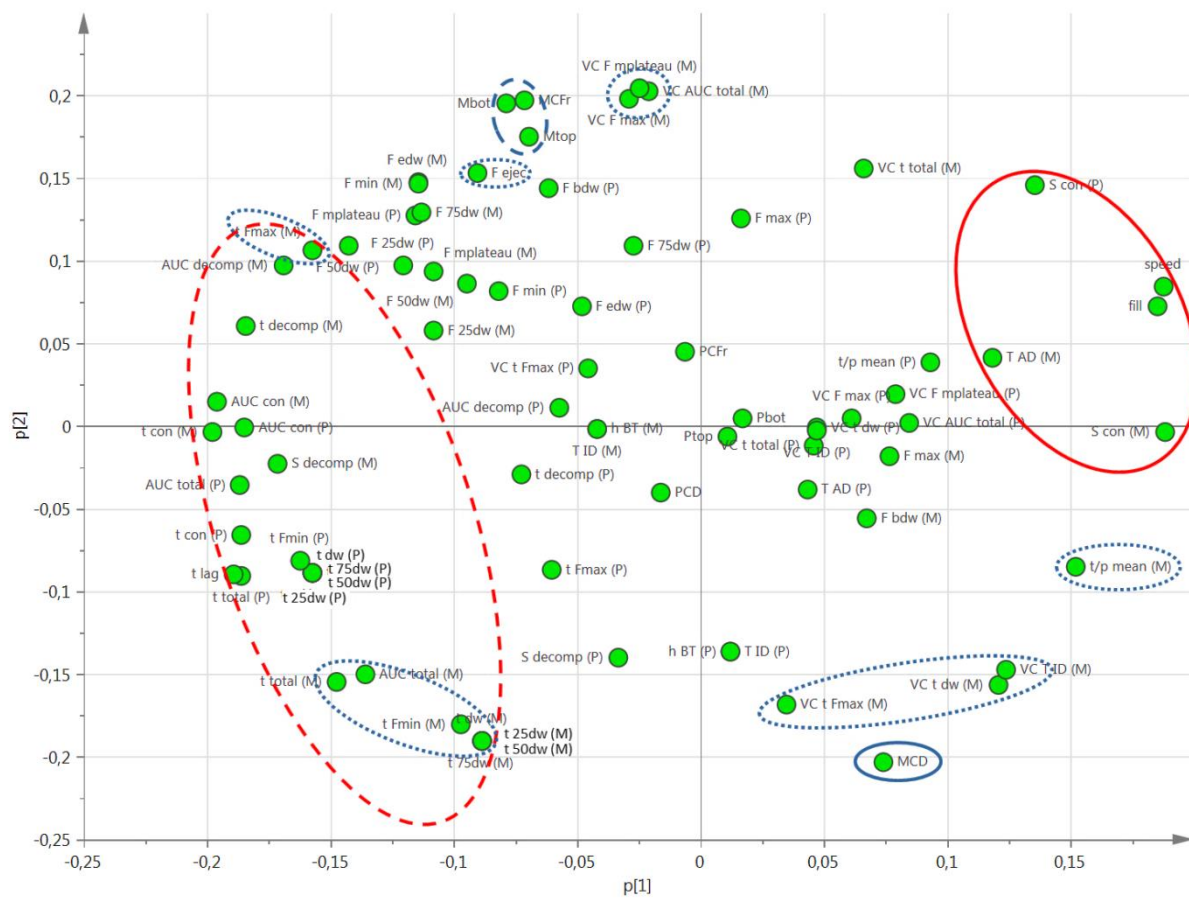


1037 Figure 8: Score scatter plot of PC1 vs. PC 2. [t1] Scores of Principal Component 1; [t2] Scores
1038 of Principal Component 2.

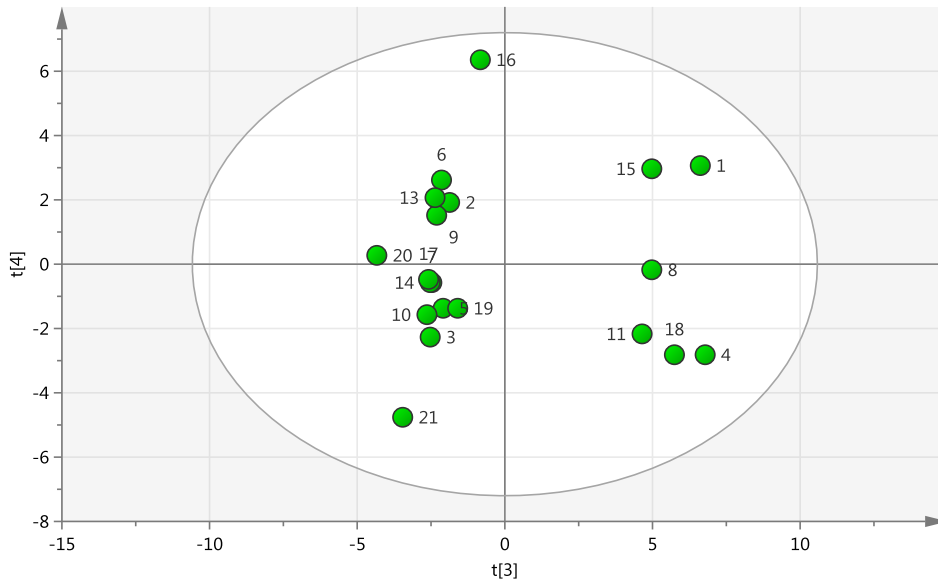


1039 Figure 9: Loading scatter plot of PC1 vs. PC 2. [p1] Scores of Principal Component 1; [p2]

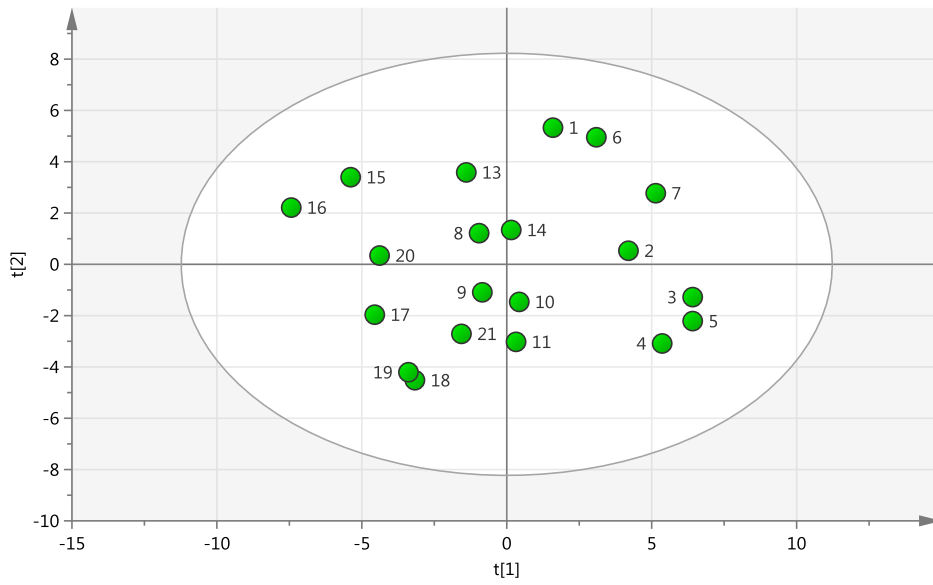
1040 Scores of Principal Component 2. Key: see Table 2 and Table 3.



1041 Figure 10: Score scatter plot of PC3 vs. PC 4. [t3] Scores of Principal Component 3; [t4] Scores
1042 of Principal Component 4.



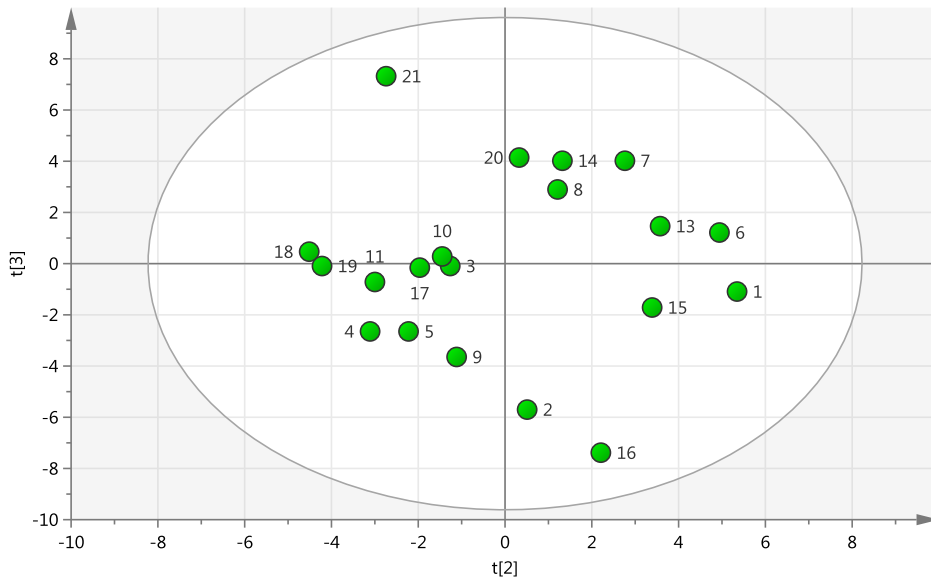
1045 Figure 12: Score scatter plot of PC1 vs. PC 2. [t1] Scores of Principal Component 1; [t2] Scores
1046 of Principal Component 2.



1047 Figure 13: Loading scatter plot of PC1 vs. PC 2. $w^*c[1]$ Loadings of Principal Component 1;
 1048 $w^*c[2]$ Loadings of Principal Component 2. Key: see Table 2, Table 3 and Table 4.



1049 Figure 14: Score scatter plot of PC2 vs. PC 3. [t2] Scores of Principal Component 2; [t3] Scores
1050 of Principal Component 3.



1051 Figure 15: Loading scatter plot of PC2 vs. PC 3. $w^*c[2]$ Loadings of Principal Component 2;

1052 $w^*c[3]$ Loadings of Principal Component 3. Key: see Table 2, Table 3 and Table 4.

